Geosci. Model Dev. Discuss., https://doi.org/10.5194/gmd-2018-66
Manuscript under review for journal Geosci. Model Dev.
Discussion started: 20 March 2018

Geoscientific Model Development Discussions

An EC-Earth coupled atmosphere-ocean single-column model (AOSCM) for studying coupled marine and polar processes

Kerstin Hartung [1,2,3], Gunilla Svensson [1,2,3], Hamish Struthers [4,5], Anna-Lena Deppenmeier [6], and Wilco Hazeleger [6,7]

[1]Department of Meteorology, Stockholm University, Sweden

[2]Bolin Centre for Climate Research, Stockholm University, Sweden

[3]Swedish e-Science Research Centre, Sweden

[4]NSC, Linköping, Sweden

[5]Linköping University, Sweden

[6]Wageningen University, The Netherlands

[7]Netherlands eScience Center, The Netherlands

Correspondence: Kerstin Hartung (kerstin.hartung@misu.su.se)

Abstract. Single-column models (SCM) have been used as a tool to develop numerical weather prediction and global climate models for several decades. SCMs decouple small-scale processes from large-scale forcing and thus allow to test physical parameterizations in a controlled environment with reduced computational cost. Typically, either the ocean, sea-ice or atmosphere is fully modelled and assumptions have to be made on the boundary conditions from other subsystems, adding a potential source of errors. Here, we present a fully coupled atmosphere-ocean SCM (AOSCM), including sea-ice, which is related to the global climate model EC-Earth, consisting of NEMO3.6, LIM3, OpenIFS cycle 40r1, and OASIS3-MCT.

The AOSCM is tested at three locations: the tropical Atlantic, the midlatitude Pacific and the Arctic. At all three locations in-situ observations are available for comparison. Evaluating model performance with buoy data, soundings and ship based observations, we find that the coupled AOSCM can capture the observed atmospheric and oceanic evolution. Model evolution is sensitive to the initial conditions and forcing data imposed on the column. Coupling several model components while alongside using them individually can help disentangle model feedbacks. Although the model can be extended, we demonstrate that already in the current setup it is a valuable tool to advance our understanding in marine and polar boundary layer processes and the interactions of their coupled components.

Geosci. Model Dev. Discuss., https://doi.org/10.5194/gmd-2018-66
Manuscript under review for journal Geosci. Model Dev.
Discussion started: 20 March 2018

Geoscientific Model Development Discussions
Open Access
EGU

1 Introduction

Single-column models (SCM) have already been used for several decades to advance our understanding of physical processes and their parametrizations in numerical models. SCMs originated from bulk (mixed-layer) models (Kraus and Turner, 1967; Niiler and Kraus, 1977). The first vertically resolved SCMs were developed in the late 1980s. For example, Betts and Miller (1986) demonstrated added value of an atmospheric SCM framework for the development and evaluation of a convective adjustment scheme in atmospheric models and Price et al. (1986) used an ocean SCM to study the diurnal cycle of the mixed layer in the subtropical Pacific. Research with SCMs is a valuable addition to studies with three-dimensional numerical weather prediction (NWP) models and global climate models (GCM). By zooming into a single grid column of a host model, either in the atmosphere, the ocean, or the sea-ice, one achieves a separation between resolved large-scale processes and processes parametrized in the vertical column. This means that physical processes, and the ability of their associated parametrization schemes to produce the correct physical tendencies, can be studied in a controlled framework (Randall et al., 1996). Similar to the setup of a three-dimensional model, initial conditions are provided, typically from a sounding, mooring or a reanalysis profile. Though the column is decoupled from the large-scale flow, forcing mimicking the influence of the large-scale circulation on the column of interest can be applied. In practice, this is done by applying pressure gradient forcing via the geostrophic wind, horizontal advection and vertical velocity forcing to the atmospheric component of the SCM. Relaxation (nudging) is an alternative way to include forcing by the large-scale environment. All forcing types can be used individually and complementary. In the controlled environment of an SCM, the evolution of idealized or realistic initial profiles exposed to forcing of varying complexity can be studied in an Eulerian or Lagrangian setting. The choice of experimental setup will affect the possibility to study the performance of different physical parametrizations. Thus, an experiment needs to be designed carefully depending on the underlying scientific question. Furthermore, by only evolving a single grid column the computational cost is reduced considerably compared to experiments with a three-dimensional model. This allows for comprehensive parameter testing as more sensitivity experiments can be carried out at much reduced time cost. In summary, an SCM can be a powerful tool if its limitations are handled with care.

For these reasons SCMs have regularly been employed to investigate physical processes. In the ocean, single-column models, sometimes just called column models, started off as bulk mixed-layer models (Kraus and Turner, 1967; Price et al., 1986). From the start they were used to study the impact of air-sea exchange and vertical mixing on the temporal evolution of the oceanic mixed-layer. In Gaspar et al. (1990) and Large et al. (1994), these bulk models are extended to 1D turbulence models which can be applied in the whole column and are thus suitable for GCMs. More recent examples of oceanic SCM models being used for model development are Ling et al. (2015) and Reffray et al. (2015).

In addition to research with individual atmospheric SCMs (e.g. Betts and Miller, 1986; Randall et al., 1996), SCM intercomparison studies have focused on e.g. convection (e.g. Betts and Miller, 1986; Ghan et al., 2000; Bechtold et al., 2000; Lenderink et al., 2004), stratocumulus (e.g. Bretherton et al., 1999; de Roode et al., 2016) and mixed-phase clouds (e.g. Klein et al., 2009; Pithan et al., 2016), and the representation of the boundary layer (e.g. Cuxart et al., 2006; Baas et al., 2010; Svensson et al., 2011, as part of GABLS (GEWEX Atmospheric Boundary Layer Study, Holtslag, 2006)). These studies also present a wide

Geosci. Model Dev. Discuss., https://doi.org/10.5194/gmd-2018-66
Manuscript under review for journal Geosci. Model Dev.
Discussion started: 20 March 2018

range of numerical approaches to set up, e.g. idealized or based on measurements, and force the model, e.g. whether Eulerian or Lagrangian forcing is prescribed. Idealized model setups are commonly complemented by large eddy simulations (LES) or cloud-resolving models (CRM) capturing the atmospheric evolution in more detail. LES and CRM are used to compile forcing data or as benchmarks when evaluating the performance of parametrization in SCMs (e.g. Bechtold et al., 2000; Guichard et al., 2004; Beare et al., 2006). The cases developed within GCSS and GABLS, which merged into GASS (GEWEX Global Atmospheric System Study) at the end of 2010, have been successfully used to identify and improve parametrized processes (e.g. Lenderink et al., 2004) and serve as testbeds for model development. 44% of modelling centres polled by Hourdin et al. (2017) reported the use of SCMs for model development and tuning. This coordinated way of working has not been, to our knowledge, as extensively utilized in the ocean or sea-ice communities.

In contrast to global climate models, SCMs have mostly been implemented uncoupled. Thus, for the majority of studies mentioned, the surface is prescribed by boundary conditions. Sensitivity to the formulation of the surface boundary conditions and surface forcing (e.g. surface temperature, surface fluxes or surface energy-budget equation) was found in several of the atmospheric SCM studies. Firstly, there are theoretical limitations: while an atmospheric convective boundary layer may be forced by surface fluxes, a stably stratified one should not (Basu et al., 2008). Furthermore, a prescribed surface temperature has proven to lead to very different energy content in the boundary layer (Svensson et al., 2011) while using different land models also introduces spread (Bosveld et al., 2014 and GABLS4), a subject that is currently further studied in DICE (http://appconv.metoffice.com/dice/dice.html). Over sea-ice the presence of snow modulates the surface energy budget and thus results vary depending on the description of snow in the surface model (Pithan et al., 2016). In the ocean the depth of the mixed layer is sensitive to the coupling, especially in the tropics and during summer, when the mixed layer is shallow and quickly responding to forcing. The fast response can give rise to positive feedbacks between model biases in the atmospheric and oceanic mixed layers (Breugem et al., 2008; Toniazzo and Woolnough, 2014). It is common to develop model components using idealized forcing, i.e., ocean and land models use near-surface observed or reanalysis mean state variables to provide atmospheric fluxes. However, this can lead to surprises when model components are interactively coupled. Atmospheric models are forced with observed SSTs over the ocean and often developed in a framework with an interactive land model over land, although the land model is taken as is and i.e. thus not developed in the interactive framework. To avoid ambiguities arising from specifications of surface boundary conditions, it is desirable to combine several SCMs to one coupled model, especially when studying boundary layer processes or processes that depend on interfacial coupling.

In the last two decades a few coupled single-column models have been developed. Clayson and Chen (2002) coupled an atmosphere and an ocean SCM to study tropical atmosphere-ocean feedbacks and Goyette and Perroud (2012) combined a 1D lake model with an atmospheric column model. More recently, West et al. (2016) coupled a one-dimensional sea-ice and an atmospheric column model to investigate the optimal interface at which to calculate the surface energy budget.

Following this line of work, we present a coupled atmosphere-ocean sea-ice SCM (AOSCM) following the global climate host model EC-Earth (Hazeleger et al., 2010, 2012). The AOSCM provides a platform to study coupling processes, both physical and numerical, at the marine and polar surface interface. First, we present and discuss ways to set up and force the model. This encompasses idealized and realistic initial conditions and forcing, Eulerian and Lagrangian setups, short-term case

Geosci. Model Dev. Discuss., https://doi.org/10.5194/gmd-2018-66
Manuscript under review for journal Geosci. Model Dev.
Discussion started: 20 March 2018

Geoscientific Model Development Discussions

based or long-term statistical analysis. Application of the AOSCM is demonstrated at three locations, namely mid-latitudes, tropics and the Arctic. Varying experimental designs display the versatility of the tool.

2 Model, model setups and data

2.1 Model components

In this study, the AOSCM is realized by combining the atmospheric model OpenIFS (Open Integrated Forecasting System, https://software.ecmwf.int/wiki/display/OIFS/Single+column+model+40r1+release+notes), including the land model H-Tessel (Balsamo et al., 2009), and the ocean model NEMO (Nucleus for European Modelling of the Ocean, https://www.nemo-ocean.eu/) including the sea-ice model LIM (Louvain-la-Neuve Sea Ice Model, http://www.climate.be/repomodx/lim/index.php?id=49). All coupling actions between the column versions of the sub-components NEMO and OpenIFS are performed by the coupling software OASIS3-MCT. For model development purposes the column model should follow the specifications of a GCM host model. In an iterative process, findings from the SCM, and specifically their impact on the large-scale circulation, can then be directly tested and evaluated in the GCM. In this way the computational cost for coupled model development is reduced. Here, the AOSCM is set up to closely match the development version of the EC-Earth model. Presently, this means that the default setup is a column version of EC-Earth v3, except that instead of using IFS cycle 36r4 the AOSCM uses OpenIFS cycle 40r1. Future versions of EC-Earth will be based on OpenIFS. The other components, namely NEMO3.6, LIM3 and OASIS3-MCT, are used with the same version in both EC-Earth v3 and the AOSCM.

2.1.1 OpenIFS

OpenIFS (hereafter OIFS) is developed by the European Centre for Medium-Range Weather Forceasts (ECMWF) as a version of IFS intended for research and education (Day et al., 2017). The main difference of OIFS40r1 to IFS 40r1 is the exclusion of the data assimilation component of IFS. Extensive documentation is available for IFS at: https://www.ecmwf.int/en/forecasts/documentation-and-support/changes-ecmwf-model/cycle-40r1/cycle-40r1.

The atmospheric part of the AOSCM solves the one-dimensional version of the primitive equations:

$$-\dot{\eta}\frac{\partial u}{\partial \eta} + F_u + f(v - v_g) + P_u + \frac{u_r - u}{\tau} = \frac{\partial u}{\partial t} \quad (1)$$

$$-\dot{\eta}\frac{\partial v}{\partial \eta} + F_v - f(u - u_g) + P_v + \frac{v_r - v}{\tau} = \frac{\partial v}{\partial t} \quad (2)$$

$$-\dot{\eta}\frac{\partial T}{\partial \eta} + F_T + \frac{RT\omega}{c_p p} + P_T + \frac{T_r - T}{\tau} = \frac{\partial T}{\partial t} \quad (3)$$

$$-\dot{\eta}\frac{\partial q}{\partial \eta} + F_q + P_q + \frac{q_r - q}{\tau} = \frac{\partial q}{\partial t} \quad (4)$$

A two-time level semi-Lagrangian scheme is used (as in the full model system, an Eulerian scheme is optional) to integrate the momentum with horizontal wind components u and v (Eq. (1) and (2)), thermodynamics T (Eq. (3)), moisture q (Eq. (4))

Geosci. Model Dev. Discuss., https://doi.org/10.5194/gmd-2018-66
Manuscript under review for journal Geosci. Model Dev.
Discussion started: 20 March 2018

as well as the continuity equation. The vertical coordinate is based on η levels which merge orography following σ coordinates near the surface with pressure coordinates in the free atmosphere. Here, $\dot{\eta}$ and ω are vertical velocities, in η and pressure coordinates, respectively. F_i is the horizontal advection, P_i summarizes physical parametrizations and u_r, v_r, T_r, q_r denote the reference profiles used for nudging with a time scale τ. Furthermore, f is the Coriolis parameter, u_g and v_g the horizontal components of the geostrophic wind, R the moist air gas constant, c_p the heat capacity of moist air at constant pressure and p the pressure. In addition to the atmospheric state variables (Eq. (1) - (4)), the model prognostically calculates cloud liquid, ice, rain, snow and cloud cover.

The total tendency (right-hand sides of Eq. (1) - Eq. (4)) to each prognostic variable is calculated as the sum of dynamical (first three terms on the left-hand side) and physical parametrization tendencies P_i (fourth term), possibly updated by relaxation (i.e. nudging, fifth term). The order of the left-hand side of the equation is, in a simplified way, equivalent to the sequence in which the tendencies are calculated in the model (Fig. 1). In the time-stepping loop, the dynamical tendencies are determined, mainly aggregating available prescribed forcing. The pressure gradient forcing is represented by the geostrophic wind. The third term of the heat equation captures adiabatic heating through vertical motion. Calculations of tendencies from physical parametrizations are done in the same was as in the three-dimensional OIFS. Detailed discussion of the parametrizations used for these processes, namely, the radiation, turbulence, cloud and convection parametrization schemes as well as the non-orographic gravity wave drag, orographic gravity wave drag and surface drag, can be found in the IFS documentation for cycle 40r1 (https://www.ecmwf.int/sites/default/files/IFS_CY40R1_Part4.pdf). Relaxation tendencies are calculated weighing the difference between the new state, as determined by physical and dynamical tendencies, and a reference state, with the relaxation timescale τ. All forcing is read in at forcing time steps and linearly interpolated at intermediate model steps.

Besides visualising the sequence of main routines called during an OIFS SCM run, Fig. 1 also highlights communications with other AOSCM components through the coupler and use of coupling variables in red. Coupling variables are also schematically shown in Figure 4. They enter the primitive equation system (Eq. (1) - (4)) via the surface energy balance (Eq. (5)).

$$(1-\alpha_i)R_s + \epsilon(R_T - \sigma T_{sk,i}^4) + H_i + LH_i = Q_T = \Lambda_{sk,i}(T_{sk,i} - T_1) \tag{5}$$

The energy budget is solved individually for each surface tile i, which in the coupled system are the ocean and/or sea-ice. The downward short-wave and long-wave radiations are R_s and R_T, with the tiled albedo α_i, the surface emissivity ϵ, the Stefan-Boltzmann constant σ, the skin temperature $T_{sk,i}$ and the skin layer conductivity $\Lambda_{sk,i}$. H_i is the tiled sensible heat flux and LH_i the tiled latent heat flux. Downward coupling is implemented through the surface albedo and the temperature of the upper snow, sea-ice or ocean layer T_1.

2.1.2 NEMO

NEMO is based on the thermodynamics and dynamics OPA model (Océan PArallélisé) and includes the LIM3 sea-ice component. More details of NEMO can be found in Madec (2016) and Rousset et al. (2015) describes the recent version of LIM.

Geosci. Model Dev. Discuss., https://doi.org/10.5194/gmd-2018-66
Manuscript under review for journal Geosci. Model Dev.
Discussion started: 20 March 2018

The ocean component NEMO3.6 is a primitive equation model based on the Navier-Stokes equations (Eq. (6) and (7)), the hydrostatic equation, the incompressibility equation, heat and salt conservation equations (Eq. (8) and (9)) and the equation of state.

$$-\frac{\partial}{\partial z}\nu_t\frac{\partial u}{\partial z} + fv + P_u + \frac{u_r - u}{\tau} = \frac{\partial u}{\partial t} \tag{6}$$

$$-\frac{\partial}{\partial z}\nu_t\frac{\partial v}{\partial z} - fu + P_v + \frac{v_r - v}{\tau} = \frac{\partial v}{\partial t} \tag{7}$$

$$-\frac{\partial}{\partial z}K_t\frac{\partial T}{\partial z} + \frac{1}{\rho_o c_p}\frac{\partial I(F_{sol}, z)}{\partial z} + P_T + \frac{T_r - T}{\tau} = \frac{\partial T}{\partial t} \tag{8}$$

$$-\frac{\partial}{\partial z}K_t\frac{\partial S}{\partial z} + E - P + P_S + \frac{S_r - S}{\tau} = \frac{\partial S}{\partial t} \tag{9}$$

EC-Earth v3 uses the polyTEOS10-bsq formulation, i.e. it is based on conservative state variables and provides better conservation constraints than other representations of the equation of state. That is of less importance in the 1D version, which is therefore here based on the polyEOS80-bsq equation of state. The prognostic variables in the 1D version are the tracers potential temperature T, practical salinity S, and the horizontal velocity components u and v as described in Eq. (6)-(9). Here ν_t and K_t are the vertical turbulent viscosity and diffusivity, respectively. $I(F_{sol}, z)$ denotes the penetrative part of the solar surface heat flux and E and P are the evaporation and precipitation fluxes. P_i summarize physical parametrizations and u_r, v_r, T_r, S_r again describe reference profiles to which the modelled profiles can be relaxed with a time scale τ. The terms on the left hand sides of the equation system capture the column forcing.

The general structure and work-flow in the NEMO and LIM models are summarized in Fig. 2 and 3. The main ocean integration is organized from *stp_c1d* with tracer and momentum tendencies evaluated separately. The AOSCM setting includes physical parametrizations P_i, for example describing the turbulence closure. In the standard setting the vertical mixing scheme is based on a TKE dependent eddy coefficient and a 1.5 turbulent closure for convection but other turbulence schemes are implemented in the code and can easily be selected. A Langmuir circulation parametrization is also turned on and the effect of chlorophyll for heating due to solar penetration is taken into account. Advection of tracers is not possible in the one-dimensional framework but can, in a way similar to that applied in the atmospheric model, be approximated by relaxing profiles of both tracer and momentum fields towards reference profiles. However, this procedure is not utilized in the examples presented here.

Again communications with other components during the work-flow are highlighted in red (Fig. 2). Coupling actions are performed at the beginning of the time stepping, namely receiving fields as part of the boundary condition routines, and at the end of the time stepping, when the updated SST and ice parameters are send to the atmospheric part of the AOSCM. The boundary conditions at the surface for the momentum and tracer variables are given in Eq. (10) - (13). There, $\tau_{u,v}$ are the surface wind stress components, ρ_0 is the in situ density and S_t the rate of change of the sea-ice thickness budget. Only the non-penetrative part of the net surface heat flux (see Eq. (5)) influences the temperature boundary condition.

Geosci. Model Dev. Discuss., https://doi.org/10.5194/gmd-2018-66
Manuscript under review for journal Geosci. Model Dev.
Discussion started: 20 March 2018

$$\nu_t \frac{\partial u}{\partial z} = \frac{\tau_u}{\rho_0} \tag{10}$$

$$\nu_t \frac{\partial v}{\partial z} = \frac{\tau_v}{\rho_0} \tag{11}$$

$$K_t \frac{\partial T}{\partial z} = \frac{Q_T}{\rho_0 C_p} \tag{12}$$

$$K_t \frac{\partial S}{\partial z} = \frac{(E - P - S_t) \cdot S(z=0)}{\rho_0} \tag{13}$$

LIM3, the sea-ice model embedded in the oceanic component of the AOSCM, contains a thermodynamic and a dynamic component. In its 1D version only the thermodynamic model is currently used, including the representation of subgrid-scale distributions of ice thickness, enthalphy, salinity and age. The model includes multiple sea-ice categories of different ice thickness, set to five categories as a default. A brief description of the model sub-components is given in Fig. 3.

2.1.3 OASIS3-MCT

The OASIS3-MCT coupler (Valcke, 2006) takes care of communication between the atmosphere and the ocean/sea ice components and carries out transfers and temporal transformations of variables. Regridding is not necessary since two SCMs are coupled. Coupling is performed by the *oasis_put* and *oasis_get* actions in the atmospheric and oceanic models (see Fig. 1 and 2). At every coupling step (a multiple of each model's time step) coupling variables are exchanged between the components. It is recommended to use a temporal lag between *put* and *get* actions to avoid long-waiting times of components or possible deadlocks, even in a single-column setup. In this framework, the variables are *put* a given time before the coupling timestep, usually determined by the model timestep, but only read by the receiving model (*get*) at the coupling timestep. Thus, initialization files of the coupling variables are needed at the start of the simulation.

Variable transfer between NEMO and OIFS is implemented in both directions (Fig. 4). NEMO receives from OIFS surface stress, solar radiation, longwave radiation, sensible and latent heat fluxes, the temperature sensitivity of the non-solar heat fluxes (long-wave radiation, sensible and latent heat flux), precipitation and evaporation. In the reverse direction, only the sea surface temperature is passed in ice-free conditions. In presence of sea-ice, sea-ice albedo, thickness, fraction, temperature, and snow thickness are also transferred. Sea-ice parameters are available for the different sea-ice thickness categories but the aggregated mean is transferred to the atmosphere. If sea-ice is present, some ice parameters are also coupled to the ocean model. The ocean receives, in addition to the atmospheric parameters, sea-ice fraction, thickness, temperature, and albedo. The rate of change in ice thickness is added to the mass flux received from the atmosphere, evaporation and precipitation. OASIS3-MCT allows to pass either instantaneous values of the coupling fields at the time of coupling or transform the field by means of calculating an average, maximum, minimum or sum over the period since the last coupling. As in EC-Earth v3, coupling parameters are averaged over the coupling time step.

Geosci. Model Dev. Discuss., https://doi.org/10.5194/gmd-2018-66
Manuscript under review for journal Geosci. Model Dev.
Discussion started: 20 March 2018

2.2 How to design an (AO)SCM experiment

As mentioned in Sec 1, the freedom in setting up the model initial conditions and forcing is both an advantage and a challenge when using the AOSCM. One needs to find a balance of forcing settings based on the research question to be studied. Here, we briefly present some possibilities of using the (AO)SCM.

Figure 5 shows the main options to consider when designing an SCM experiment. Firstly, the questions is if the model should be used in an idealized setting or following measurements, reanalysis or model data. In idealized simulations the vertical structure of initial conditions and forcing as well as the vertical extent of the forcing can be simplified. If no forcing is prescribed, the model column evolves in a Lagrangian way. In an SCM it would usually be assumed that the whole column is migrating simultaneously, although this is likely not true in reality. The Lagrangian approach of following an air parcel needs to be adapted in an AOSCM as disregarding relative horizontal velocities of the components is unrealistic, especially for longer simulations.

More complex experiments can be designed in a variety of ways, as for example described in Randall and Cripe (1999). They are presented here in order of increasing control on the model evolution and complexity of the setup. It is often advisable to combine several of these forcing options.

Pressure-gradient forcing is one of the most basic large-scale forcings. It ensures that energy is supplied from the non-resolved large-scale pressure field to counteract energy loss through frictional dissipation near the surface. As the wind is forced to be close to the geostrophic wind, modulated by the timscale prescribed by the Coriolis parameter, it can be understood as a physically motivated relaxation. Unless nudging of the wind is applied, this forcing is necessary and it is in general advisable for longer simulations. Forcing with geostrophic winds is known to introduce inertial-type oscillations into the column (e.g. Egger and Schmid, 1988). Advective tendencies of prognostic variables and vertical velocity also emulate the influence of neighbouring columns on the column of interest. As the vertical structure in the AOSCM might differ from the host model column or from measurements, one needs to ensure that the tendencies are physically reasonable and, if possible, prevent the model from drifting away. Thus, it might be necessary to apply advective tendencies only, or not, over a specific height interval or to add relaxation forcing. It should be noted that the vertical velocity is often corrected from large-scale forcing (Sigg and Svensson, 2004) since it is a parameter not easily diagnosed in large-scale models. For example, in ERA-Interim (Dee et al., 2011) the vertical velocity is a combination of the diagnosed vertical velocity and residuals from the calculation of physical parameterizations (Nils Wedi (ECMWF), personal communication). Finally, the model column can be forced by relaxation (also called nudging). This is the forcing option which is the most dependent on the actual model state at the time the forcing is applied and the only one which is not mimicking a process resolved in a three-dimensional model. Weighted with the characteristic time scale of relaxation the AOSCM column mean profile is forced towards a reference profile. Thus, nudging can alleviate or prevent model drift, depending on the time scale chosen. However, nudging best reduces biases of state variables and has been reported to lead to problems for variables describing rates, extensively documented for precipitation (e.g. Randall and Cripe, 1999; Hack and Pedretti, 2000; Ghan et al., 2000). Another restriction is that some physical parametrizations can only be tested if the momentum balance is not artificially altered. While the cloud micro-physics description could be evaluated

Geosci. Model Dev. Discuss., https://doi.org/10.5194/gmd-2018-66
Manuscript under review for journal Geosci. Model Dev.
Discussion started: 20 March 2018

in a AOSCM applying relaxation, a study of the boundary-layer turbulence evolution is not recommended. Nudging changes the equilibrium of dynamic forcing and physical parametrizations and might mask model biases. On the other hand, nudging tendencies can be evaluated and used to diagnose model drift and imbalances. Nudging is also useful as it allows handling of inaccurate or missing information, like inertial oscillations of wind or vertical velocity forcing.

After designing initial and forcing data, the number and length of simulations needs to be decided. Measurement campaigns are usually limited in time and thus motivate shorter simulation lengths. Even if relaxation of the profile is used to prevent model drift, the impact of initial condition and forcing sensitivity might limit the model run length to which parametrizations can be evaluated.

The physical processes of interest, and the need to appropriately resolve them, determine settings of time steps, vertical grid and coupling frequency. Even though not feasible for the host model for which settings are usually tested, it is desirable to run the SCM with highest temporal and spatial resolution. Similarly, the model can be used to develop and understand different coupling options, like asynchronous coupling (Lemarié et al., 2015), which are less feasible in a three-dimensional model.

Both pressure gradient forcing and horizontal advective tendencies are calculated based on horizontal gradients. Thus, it should be noted that when using forcing based on model data, they depend on the horizontal resolution of the host model. In addition, the temporal resolution of the forcing steers how closely the observed temporal evolution can be captured.

2.3 Experimental setup and evaluation

In this section, the setup of the AOSCM applied at three different locations, namely the Pacific midlatitudes, the tropical Atlantic and the North Polar region, is presented. We start by detailing the data used and settings common to all or most of the locations.

For all locations atmospheric initial conditions and forcing are obtained from ERA-Interim (Dee et al., 2011), though with different temporal and spatial resolution. Both analysis steps, which are provided every six hours, and intermediate 3-hourly forecast are used. The OIFS SCM is initialized with profiles of the non-cloud atmospheric prognostic variables. In case of atmosphere-only simulations, the sea surface temperature is initialized and updated daily. All forcing data, horizontal advective tendencies of the prognostic variables, geostrophic and vertical velocities, are calculated from the three-dimensional fields of ERA-Interim for each output timestep. To ensure best performance, the equivalent resolution of the ASCM is set to T511, mainly influencing the convective adjustment timescale. In contrast to EC-Earth v3, the radiation time step is equal to the dynamics time step of 900 s.

The ocean is initialized from observed daily-mean profiles of temperature and salinity measured to a depth of between 120-500 m at the marine locations. As these depths are well below the typical mixed layers, we assume that temporally coarser data in the deeper ocean does not influence the model evolution near the surface significantly. Therefore, the observed initial profiles are extended below by monthly-mean potential temperature and salinity ORAS4 fields (Balmaseda et al., 2013). At the Arctic location the initial ocean profiles are fully taken from ORAS4 data. The ocean is only forced by coupling information from the atmosphere.

Geosci. Model Dev. Discuss., https://doi.org/10.5194/gmd-2018-66
Manuscript under review for journal Geosci. Model Dev.
Discussion started: 20 March 2018

Geoscientific Model Development Discussions
Open Access
EGU

The NEMO configuration differs from the standard EC-Earth GCM settings, since it is uses NEMO-C1D options (Reffray et al., 2015). Namely, the equation of state formulation and the temporal chlorophyll structure are adapted. Instead of a constant value, SeaWIFS based chlorophyll climatologies are used (NASA Goddard Space Flight Center, 2014), based on Reffray et al. (2015) for the PAPA location. No bottom geothermal heating is parametrized and the enhanced vertical mixing schemes of EC-Earth is turned off.

2.3.1 Midlatitudes: PAPA station, east Pacific

For the first experiment we place the AOSCM at the PAPA mooring in the midlatitudinal east Pacific (nominally at $50.1°$ N, $144.8°$ W, https://www.pmel.noaa.gov/ocs/Papa). Observations at this location have been extensively used to develop physical parameterization in the ocean (e.g. Gaspar et al., 1990; Reffray et al., 2015), because the buoy is situated in a region of weak horizontal advection.

The main experiment at the PAPA location consists of a 5-day coupled atmosphere-ocean simulation, initialized on 11 July 2014 at 18 UTC (11am local time). The atmospheric model uses 60 levels and is forced with 6-hourly data (AOSCM-6h). The ocean column is resolved with 75 layers that are initialized from daily-mean profiles of temperature and salinity measured to a depth of 200 m. The coupling time step and coupling lag are chosen equal to the time step of the individual model components to be 900 s. Restart files of surface parameters required for coupled simulations are obtained from a short ASCM simulation. An uncoupled atmosphere-only simulations with 6-hourly atmospheric forcing (ASCM-6h) and a coupled simulation with 3-hourly atmospheric forcing (AOSCM-3h) act as sensitivity runs to the main setup. One further set of simulations highlights how model drift in the free troposphere can be minimized. Here, nudging of temperature, moisture, and horizontal wind with a timescale of $\tau = 6$ h above a height of 3 km is applied. In addition, the model was run with the standard setting extended by relaxing the horizontal wind with a timescale of $\tau = 1$ h. With each of the experiment settings described above, a further sixteen 29-day long simulations started at 18 UTC are run for statistical assessment.

The atmospheric column of the model is first compared with ERA-Interim to ensure that the mean large-scale state is not drifting. Surface variables are evaluated using hourly averaged PAPA mooring surface measurements. The variables used here are, with measurement error estimates in parentheses: near-surface temperature ($\pm 0.2°$ C), SST ($\pm 0.003°$ C), 10 m wind speed (± 2 %), wind-speed corrected precipitation (± 4 mm h^{-1} on 10 min filtered data with measurement threshold of 0.2 mm h^{-1}), long- and short-wave radiation (downwelling component with ± 1 % error) and turbulent fluxes of heat. Thus, the model evaluation includes both a model-model comparison and an evaluation of grid-box mean results with point-measurements. The timeseries of ocean profiles at the PAPA location are influenced by tidal oscillations. As the model does not resolve these, the oscillations in measurements are removed by applying a running mean of 12h for the comparison.

2.3.2 Tropical Atlantic

The second marine location at which the SCM is tested lies in the tropical Atlantic, situated at the 6°S, 8°E buoy of the PIRATA mooring array (Servain et al., 1998; Bourlès et al., 2008, https://www.pmel.noaa.gov/tao/drupal/disdel/). We choose a boreal summer month to demonstrate the AOSCM's ability to follow the SST cooling connected to the annual cold tongue

Geosci. Model Dev. Discuss., https://doi.org/10.5194/gmd-2018-66
Manuscript under review for journal Geosci. Model Dev.
Discussion started: 20 March 2018

development in the topical Atlantic (Lübbecke et al., 2010; Xie and Carton, 2004). During the period of 1-30 June 2014 mooring observations of SST, radiative fluxes, and ocean temperature and salinity are available for SCM evaluation. For evaluation of the experiments the observational data are complemented by ERA-Interim for the atmosphere. The ocean is initialised with daily mean temperature and salinity at the 1st of June from 0-500 m and 0-120 m respectively. We perform experiments in several settings of the AOSCM and one OSCM simulation. The atmosphere is run with 60 levels and either forced by advective tendencies and vertical velocity only (F01, F12, F15), or additionally, profiles of temperature, moisture, and horizontal wind are nudged above 1 km with a timescale of 6 hours (N1km6h). For comparison we also perform an ocean-only simulations, which is forced by hourly precipitation, near-surface wind, temperature and moisture from ERA-Interim and shortwave- and longwave radiation measured at the PIRATA buoy (OSCM). The oceanic, atmospheric, and coupling time steps are 900 s each.

2.3.3 North Polar region

To explore the AOSCM in an experimental setting with idealized forcing, and to show the additional interaction with sea ice, we choose an Arctic summer case. For this location (76° N, 160° E), we have observations from the ACSE (Arctic Clouds in Summer Experiment) campaign during a warm-air advection episode in early August 2014 causing rapid ice melt (Tjernström et al., 2015). Sotiropoulou et al. (2018) apply idealized forcing to a LES case to study the importance of advection for cloud evolution during this period. Here, we present results from the LES (Savre et al., 2014) in comparison with results from the ASCM using the same experimental setup as in Sotiropoulou et al. (2018). Furthermore, we explore the importance of coupling to the ocean/sea ice as well as the sensitivity to atmospheric model time step and coupling frequency in ASCM and AOSCM experiments. With the aim to separate the influence of local and remote processes, as in Sotiropoulou et al. (2018), we turn off large-scale advection of heat and moisture.

The idealized experiment, loosely based on observations, assumes an initial ice concentration ($100\ \%$), surface albedo (0.65) and temperature (273.15 K, i.e. melting point of ice). The LES is applying a surface friction velocity of 0.2 m s^{-1} as lower boundary condition, while it is modelled in the ASCM and AOSCM using a surface roughness, updated from its default value (0.001 m) to 0.06 m to achieve approximately the same averaged u_*. The LES and the atmospheric component of AOSCM are initialized with the same vertical mean profiles, smoothed versions of soundings at 1 August 06 UTC, the starting time of the simulation. The forcing consists of a constant geostrophic wind of 5.4 m s^{-1} and advective tendencies of temperature and humidity, all derived from 6-hourly ERA-Interim data interpolated to a vertical L137 grid but restricted vertically to the LES boundary layer height. All forcing is 6-hourly in accordance with the LES setup. The synoptic scale divergence (i.e. vertical advection), is not directly taken from the ERA-Interim as it generates unrealistic results. Thus, a prescribed divergence of $2.3 \cdot 10^{-5}$ s^{-1} is applied over the first 18 simulated hours and then decreased by $50\ \%$.

Geosci. Model Dev. Discuss., https://doi.org/10.5194/gmd-2018-66
Manuscript under review for journal Geosci. Model Dev.
Discussion started: 20 March 2018

3 Results

3.1 PAPA mooring

As a first marine test location we choose the PAPA mooring in the east Pacific. Results are presented from one short summer case study and from 16 month-long simulations distributed throughout the year.

3.1.1 Case study

During 11-15 July 2014, the PAPA mooring briefly experienced an atmospheric cold advection event, followed by a period of weak advection, which was finally ended by warm advection (not shown). A cloud, which initially caps the boundary layer, rises and dissipates after about two days. Only during the last day does a cloud form again, associated with the warm advection.

AOSCM-6h reproduces the general temporal evolution as given by the forcing, but shows a mismatch in cloud height of up to 500 m, associated with temperature and moisture biases (Fig. 6 a and b). Modelled temperatures are overestimated at and below the reanalysis cloud height and are underestimated above, with cold biases peaking at the height of the modelled cloud. In addition, the AOSCM produces too much water vapour mixing ratio relative to ERA-Interim. In the reanalysis, the cloud dissipates during 13 July whereas at least a thin cloud is persisting for most of the simulation time in the three model experiments. The atmospheric boundary layer height varies around 500 m and the marine turbocline stays shallow, reaching at most 20 m (Fig. 6c). Atmospheric evolution and biases are similar in AOSCM-3h and ASCM-6h.

Figure 7 summarizes the comparison between the modelled surface parameters and the PAPA measurements. If the model forcing is updated less frequently (A(O)SCM-6h), oscillations in the wind arise with larger amplitude than in AOSCM-3h (Fig. 7f). Oscillations occur mainly during periods of weak wind forcing and their amplitude increases with height (not shown). They are a sign of the column not being in geostrophic equilibrium and are enhanced if applying pressure gradient forcing, as this adds momentum to the column. A footprint of the artificial inertial oscillations is visible in the boundary layer height (Fig. 6a) and the turbulent surface fluxes (Fig. 7d, e). The flux oscillations arise from the oscillating near-surface shear, which generates turbulence. In the coupled simulations, temperature biases peak around 1° C (Fig. 7a, b). In ASCM-6h a larger 2m-temperature bias can be reduced to similar values if forced with observed hourly SST instead of daily mean SST from ERA-Interim (not shown).

Comparing AOSCM-6h results to reanalysis data and PAPA measurements reveals disagreements in terms of bias signs. On the one hand, the reanalysis, and thus the forcing state, indicates that the AOSCM is too warm and moist near the surface. On the other hand, comparison to PAPA measurements points to an underestimation of atmospheric moisture (too large upward latent heat flux) and too cold near-surface temperatures. These differences might partly be explained by deviations in the SST between reality and ERA-Interim reanalysis, which steer boundary layer dynamics via stability differently. It is interesting to note that when the atmospheric evolution is nudged to tightly follow the reanalysis, the cloud structure, as well as short- and long-wave radiation compared to measurements, improve. Near-surface temperature and latent heat flux, however, deviate even further from observations. During the studied period, the AOSCM captures the local observations even with the likely erroneous large-scale forcing. Comparison with the large-scale forcing fields can be used to reveal potential atmospheric model

drifts. However, in ERA-Interim the coupling to the ocean is not interactive and SSTs are only prescribed with daily resolution. One way to overcome this is to use measurements for the analysis since they reflect the observed coupling and are dependent on the true near-surface stability.

The evolution of the atmosphere is sensitive to the initial conditions. Initializing the model only six hours later increases the biases during the final warm air advection period. In this simulation the cloud cover is underestimated, thus giving increased biases in the radiative fluxes at the surface. Furthermore, in this setup a strong sensitivity to forcing frequency can be diagnosed, as these biases do not occur in AOSCM-3h results. Again, nudging the wind down to the surface removes the cloud biases. Initializing 18 hours earlier, on the other hand, does only weakly influence the results.

3.1.2 Statistical assessment

A set of root mean square error (RMSE) statistics summarizing results of sixteen simulations for the main three setups AOSCM-6h, ASCM-6h and AOSCM-3h is presented in Tables 1 and 2. Statistical significance is assessed by testing two mean values and their range of one standard deviation to be disjoint. Results are separately compiled for warm and cold periods (not shown in the tables, only in Fig. 8) with eight of the sixteen simulations falling into each category. Here, warm cases are characterised by a mean ocean mixed-layer depth of less than 10 m (November-April) and cold cases by more than 30 m (June-September).

AOSCM-6h and ASCM-6h exhibit similar monthly mean biases in the considered parameters. Daily-mean SSTs used to force ASCM-6h simulations are one-sided statistically significantly superior to SSTs modelled by the AOSCM-6h. Reduced variability is due to a coarser temporal resolution of the forcing. The signal is largest in summer months and can be explained by SST cold biases in AOSCM runs, in some cases also present during winter. This SST bias in AOSCM is part of a temperature bias dipole in the ocean column which intensifies with runtime. Reffray et al. (2015) discuss a sensitivity of the mixing depth to a TKE length parameter describing the deepening of the mixed layer by near-inertial waves and ocean swell or waves. In the standard TKE setup used in EC-Earth v3, the parameter is either a function of latitude and set as 30 m at the PAPA station (standalone ocean model) or set to 0 m so that no additional mixing is supplied (coupled model). Setting the parameter to 0 m, thus not considering additional mixing by waves, produces very similar results to the ones presented here (Tables 1 and 2), but cold biases during summer months are now replaced by warm biases of roughly equal strength and too shallow mixed layers (not shown). Reducing the value of the parameter to 10 m, as suggested by Reffray et al. (2015), and thus limiting an increase of mixing depth by internal mixing, alleviates the observed summer cold biases (not shown).

In general, the AOSCM can successfully reproduce atmosphere-only results. The added benefit of a coupled simulation is that the interactions between the marine and atmospheric boundary layer are resolved and can be studied directly. AOSCM-3h, forced with atmospheric data of higher temporal frequency, is better able to represent measurements and model reference data than AOSCM-6h, with largest impact on momentum. Again the annual mean signal originates mainly from one subperiod, in this case the cold months, when AOSCM-3h performance exceeds that of AOSCM-6h in several aspects. Firstly, wind biases are statistically significantly reduced in the whole atmospheric column. Secondly, the mean column state bias is reduced, although not statistically significantly. In addition to improvements in the mean state, an increase in the depth of the mixed layer is found in both atmosphere and ocean (not shown), related to reduced coupling biases, though not statistically significant.

Geosci. Model Dev. Discuss., https://doi.org/10.5194/gmd-2018-66
Manuscript under review for journal Geosci. Model Dev.
Discussion started: 20 March 2018

Higher frequency forcing is in many cases linked to pronounced improvements in wind representation through reduction of oscillations in wind speed. One way of emulating this effect is to relax horizontal wind profiles in the model towards those provided by reanalyses. Results from simulations applying wind relaxation over the whole column with a timescale of 1 h are summarized in the 4th columns of the tables 1 and 2. Atmospheric column and surface wind biases can be reduced by nudging the wind, as well as SST biases alleviated during cold months (not shown). Atmospheric temperature and humidity biases are not sensitive to wind nudging. However, the ocean is affected through momentum transport during cold months. The ocean responds similarly as in AOSCM-3h simulations, though only one-sided statistically significant. The ocean mixed layer is deepening whereas the annual mean atmospheric boundary layer is shallower than in all other configurations. Thus, nudging of the wind components can be used to reduce model biases. However, it has to be noted that wind nudging perturbs the momentum balance. Especially when studying boundary layer turbulence parametrization, nudging interferes with the performance of the parametrization.

In some simulations the free troposphere drifts away from the reanalysis state. A weak atmospheric nudging of the four main prognostic variables temperature, moisture and horizontal wind above 3 km (i.e. well above the boundary layer) reduces biases in the troposphere even below 3 km (Table 2). At the same time, the ocean state is only weakly influenced by deepening the ocean mixed layer. This way of nudging can be used even when the momentum balance at the surface is required to be unperturbed in the boundary layer.

Accumulated energy fluxes and accumulated precipitation from the main three sensitivity runs are visualized in Fig. 8, resolving individual cases. Modelled fluxes are sampled every hour to match the measurement frequency. In summary, the surface receives too little energy in the model during summer and loses too much energy during winter. Considering all seasons, AOSCM-3h/6h perform best compared to ASCM-6h but the main signal appears in different seasons. AOSCM-3h gives the best net surface energy balance during summer and during winter AOSCM-6h exceeds the other setups. However, the overall variability is large and individual cases may show different results. Precipitation is larger during winter and the model produces generally more rain than observed.

3.2 Tropical Atlantic

Our second marine test location is the tropical Atlantic. During the time of the case study, June 2014, SSTs in this area cool by 4 °C. This trend is part of the cooling of the eastern tropical Atlantic due to its annual cycle (Lübbecke et al., 2010; Xie and Carton, 2004). To estimate AOSCM performance in this region, we perform a base simulation using only advective tendencies (F01 in Fig. 9). Within ten days, two main biases develop, one atmospheric and one oceanic. Firstly, temperatures between 0.5 km and 1.5 km are overestimated, while moisture is underestimated over the same height interval (not shown). The patterns of these atmospheric biases are closely correlated and peak between June 14 and 17. Both biases are flow-dependent, i.e. they are not connected to a model drift but reduce again after the June 17. The integrated bias (RMSE) in the lower 1.5 km develops similarly for temperature (Fig. 9a) and moisture (not shown). Secondly, although the cooling of the ocean surface layer is partly captured, its amplitude is underestimated, leading to a warm bias of around 2°C at the end of the simulation (Fig. 9b). It is worth noting that the ocean column follows the observations well until five days into the simulation, when the observed ocean

Geosci. Model Dev. Discuss., https://doi.org/10.5194/gmd-2018-66
Manuscript under review for journal Geosci. Model Dev.
Discussion started: 20 March 2018

cooling can no longer be matched by the model. The SST bias grows, and after a short period of recovery around day 7 to 10, it increases during the course of two days and does not reduce significantly afterwards. Emergence of a model warm bias during the build up of SST cooling is a common model bias in the tropical Atlantic (Breugem et al., 2008; Toniazzo and Woolnough, 2014; Voldoire et al., 2018).

We demonstrate how the origins of the two biases can be traced in several sensitivity experiments. Nudging above 3 km, as done in the PAPA case, also reduces the near surface bias in moisture and temperature, but in a weaker form (not shown). The atmospheric bias can largely be alleviated by nudging prognostic variables above 1 km with a time-scale of τ =6 h (N1km6h). However, the SST evolution is not influenced by atmospheric relaxation to a height of 1 km. Inspired by the indication of a flow dependent bias in the standard setup, F12 and F15 show simulations with the same setup as F01 but initialized at days 12 and 15, respectively. Initializing the ocean between June 10-15, when the largest SST bias develops, strongly improves the SST representation in the AOSCM. The atmospheric biases develop again, stronger in F12 than in F15.

Finally, the SST bias can be studied by decoupling the ocean from the atmosphere. This can either be done by nudging the atmospheric column strongly (e.g. $\tau = 0.25$ h) down to the surface (not shown) or by performing an ocean-only simulation (OSCM, Fig. 9b). Both simulations produce very similar evolutions of the SST bias (not shown). The similarities point to an oceanic origin of the SST bias, while differences to F01 indicate the impact of additional feedbacks on the bias development. Observations of the ocean current vector (available at 10 m depth during this period) indicate two maxima of about 50 cm s^{-1} at June 5 and June 10 (not shown), coinciding with periods of maximum SST bias in all simulations initialized at June 1. The ocean model currently does not capture horizontal temperature advection. Temperature changes related to advection hence cannot be reproduced by the SCM. Heat budget analyses shows these terms to be small in the region of the experiment (Giordani et al., 2013; Deppenmeier et al., 2018). However, short time scale events are likely to be missed and can impact the budget on shorter times. Another possible oceanic origin of the bias is insufficient ocean vertical mixing of near-surface warming into the ocean. The importance of and sensitivity to vertical ocean mixing has been observed and demonstrated by Hazeleger and Haarsma (2005) and Hummels et al. (2013), among others. Too little mixing of cold water masses into the well-mixed layer as well as too little heat transport from the upper layer into the ocean leads to artificially warm SSTs, similar to those observed towards the end of the simulation. In the current setup, upper ocean vertical mixing only penetrates the first upper meters of the ocean column, and then stops abruptly. Replacing the relatively strongly stratified observed profile with the more gradual profile from ORAS4 deepens the mixed-layer slightly, but still only down to 20 m (not shown). This feature and its impact on the SST evolution are currently under investigation.

3.3 North Polar region

Finally, the AOSCM is used to simulate a moist intrusion event in the Arctic summer. Figure 10 shows the evolution of the liquid-water content for the reference LES simulation (a) together with observational estimates of cloud top and different versions of the ASCM and AOSCM (b-f). The atmosphere only run (b) is the most similar to the LES as it keeps a cloud with a top at about 200 m during the whole simulation. The formation of the cloud in the beginning of the simulations (not shown) is quite different. The LES initially forms a cloud with a top at about 800 m that is slowly descending under the influence of

Geosci. Model Dev. Discuss., https://doi.org/10.5194/gmd-2018-66
Manuscript under review for journal Geosci. Model Dev.
Discussion started: 20 March 2018

the subsidence. In all the AOSCM simulations, a cloud also forms at that height, dissipates and after a few hours a new cloud appears with a top at around 200 m. The evolution of the simulated cloud between hour 12 and 48 is diverging from a similar state at around hour 12 with sensitivity to coupling and time-step. In a simulation with short timesteps in all model components and coupling at every time step ($\tau = 450$ s, Fig. 10.c) the cloud develops into a double-layered cloud at about hour 32. Using a longer time-step, 2700 s as is used in EC-Earth (Fig. 10.d), results in a descending and thinning cloud, which at the end of the period is only present close to the surface. Returning to a shorter time-step of 900 s in the atmosphere but keeping the ocean, ice and coupling at 2700 s, results in a cloud that keeps its top at 200 m for a longer time (Fig. 10.e). Two simulations are run where first the temperature and then the moisture advection is turned off, the resulting cloud for the first simulation is not that different (compare Fig. 10.e and f). When the moisture advection is removed, the cloud disappears before hour 12 (not shown).

The integrated liquid-water content between hour 12 and 48 is presented in Fig. 11. The LES liquid water path (red) varies between 50 and 150 g m^{-2} during the simulation, while the observations show a wider range. Only the ASCM (blue dashed line) reaches observed values, the coupled simulations (thick lines in blue, magenta and cyan) produce smaller liquid water paths and little variability in sensitivity tests. In this figure, the importance of advection of moisture is clearly seen (dash-dotted cyan line, near the bottom of the figure). Without temperature advection (cyan dashed line) the cloud stays cooler and can thus hold more liquid water.

For this Arctic case, the cloud both shields the surface from the sun and increases the long-wave radiation. For the short-wave cloud effect, the surface albedo plays an important role. As discussed in Tjernström et al. (2015), the surface is changing characteristics rapidly as energy is absorbed and melting occurs. Figure 12 shows the initial albedo in the simulation (averaged over hour 1) for the various simulations calculated using the model's incoming and reflected shortwave radiation. The albedo during the first hour is a result of both the initialization (same for all coupled simulations) and processes changing the albedo. The albedo in the AOSCM is calculated in LIM based on the sea-ice state and is quite different from the default albedo climatology provided to the ASCM. In the coupled simulations the albedo spans from about 63 to 74 %, while the ASCM's albedo is at 58 %. The LES value is 65 % and constant in time. Some of these differences can be explained by how the cloud affects the diffuse radiation and thereby the amount of reflected light at the surface. The albedo decreases over the 48 hours in all simulations, the most (≥ 15 %) in the simulation where the cloud disappears. This illustrates the complexity of the coupling and all these processes influence the net energy received by the surface.

In Fig. 13, the net mean energy at the surface, with and without the sensible and latent heat flux contribution, is shown. The deviation from the dashed 1-to-1 line gives the magnitude of the turbulent fluxes. In all simulations, the turbulent fluxes present a net source of energy for the surface i.e. stably stratified conditions dominate. However, the observational estimate (black dot) shows a small net upward flux and the overall available energy at the surface is about 40 W m^{-2} less. This analysis points to differences in the vertical structure of the atmosphere.

Geosci. Model Dev. Discuss., https://doi.org/10.5194/gmd-2018-66
Manuscript under review for journal Geosci. Model Dev.
Discussion started: 20 March 2018

4 Summary and outlook

We demonstrate a coupled atmosphere-ocean single-column model (AOSCM) following the setup of the next version climate model EC-Earth (Hazeleger et al., 2010). The AOSCM is designed for studying the physical interaction of oceanic and atmospheric boundary layer processes as well as technical aspects of the coupling. Here, we demonstrate the functionalities of the model by applying it at three locations and present analysis showing the versatility of the tool. Furthermore, we highlight avenues of how to design process studies using the AOSCM.

The AOSCM reproduces the evolution of the Earth system column and can simulate it reliably during short and month-long experiments. We demonstrate the model at three different locations, with varying degree of forcing complexity, in a framework with coupled and individual model component simulations. Based on results from the PAPA station and considering atmosphere-only setups as a benchmark, the AOSCM is performing well and is in some cases even superior to the ASCM (atmosphere single-column model). Extending an ASCM to an AOSCM allows us to resolve coupled processes. A sensitivity to the forcing frequency is apparent, which is largely related to deteriorated winds in simulations forced with infrequent data. Both the horizontal advection and the vertical wind forcing are captured more realistically with increased forcing frequency. It should be noted that a linear interpolation will result in deteriorated results even for perfect forcing data. A linear functionality is likely not a good assumption for the temporal evolution of the forcing fields. Wind components can be nudged to alleviate oscillations in wind speed, while this process does not influence temperature and moisture evolution. Nudging wind down to the surface ensures that atmospheric momentum biases do not deteriorate ocean performance but the nudging interferes with parametrizations connected to momentum, e.g. turbulence. Nudging all fields above the boundary layer with weak nudging time scale remedies biases in the free troposphere while allowing to focus on the freely evolving surface interactions. At the PIRATA buoy nudging above 3 km also reduces time-dependent atmospheric biases considerably. Biases are almost completely removed when reducing the lowest nudged height to 1 km. At the sea surface, a temperature bias remains even in an ocean-only setting or with a strongly nudged atmosphere. Both biases are sensitive to initialization time of the simulation. The sensitivity tests performed for the Arctic case, compared with both observations and an idealized LES simulation, show the complexity of how the coupling between the lower atmospheric structure, surface properties and clouds affect the energy budget at the surface. Further analysis of this case is ongoing.

Based on our results we recommend to force the AOSCM with advective tendencies and pressure gradient forcing in the atmosphere. The forcing frequency should be kept as short as possible, ideally based on information from the host model at every time step, e.g. for model development. If model drifts or other persistent biases are identified, nudging profiles down to the surface or above the processes of interest can be added to enhance stability of the simulation and keep close analogies with observations. Running several sensitivity experiments based on different forcing and coupling settings, periods for further parameter sensitivity experiment can be identified and then studied inexpensively in the AOSCM.

As the AOSCM consists of individually compiled components it is relatively straightforward to update and exchange routines, e.g. when newer cycles become available. At this stage the capabilities of the EC-Earth AOSCM can be extended along several avenues. Even though the hydrometeorological variables cloud liquid, ice, rain, snow and cloud cover are treated prog-

nostically in OIFS their profiles can currently not be forced by advective tendencies or nudging. The missing advection terms can be partially included by adding the advective tendencies of cloud liquid and ice mixing ratios to the advective tendency of water vapour mixing ratio. Similarly, advective tendency forcing could be added to both the sea-ice and ocean equation systems. Apart from the necessary model infrastructure, this requires observations or model data to compile the relevant forcing. With the current model without advective forcing, one option is to limit the run time of the model. In that case the relative stationarity of ocean and sea-ice relative to atmospheric movement can be assumed. The other option is to relax the ocean profile towards a reference profile, either across the whole column or only below the mixed layer. A similar feature, namely an adaptive relaxation height, is currently not available in the atmospheric part of the AOSCM. It is however possible to nudge only above a constant level, as we demonstrate. If chosen well above the boundary layer, this still ensures that the boundary layer is not affected by nudging while biases in the free troposphere are limited.

Even though the model can be extended in numerous ways it is a useful tool to explore several open science questions already at the current stage. A non-extensive list of problems that can be tackled includes:

In the marine environment simulations similar to ASTEX (Bretherton et al., 1999; de Roode et al., 2016), describing stratocumulus to cumulus transition, can be performed with coupled models. Independent of the location where it is placed, a coupled atmosphere-ocean SCM allows to study the concept of stochastic air-sea fluxes decoupled from large-scale motions (Williams, 2012). An AOSCM, including sea-ice, presents the opportunity to study physical processes in the polar regions. The atmosphere-ice-ocean system is strongly coupled and sensitive to even small energy imbalances at the interfaces and thus to the correct representation of sea-ice fluxes (Bourassa et al., 2013; Spengler et al., 2016). Understanding of the processes relevant for sea-ice melting and freeze-up in the changing polar regions is crucial. Work can be done along the lines of previous studies, like Pithan et al. (2016), investigating Arctic air mass transformations, and the local interactions with the snow surface (Sterk et al., 2013; Lecomte et al., 2015).

The AOSCM is a tool for investigating interactions at the air-ice-ocean interface. It can yield insights into the physical processes responsible for model shortcomings in areas where the coupling at the interface plays a considerable role. With its low computational cost it can help understand how choices of coupling parameters and numerical setup influence the evolution of the whole column.

5 Acknowledgements

We would like to thank for support from (O)IFS, OASIS, NEMO and LIM communities. In addition we would like thank ECMWF for providing ERA-Interim data and support compiling forcing information, especially Nils Wedi, Filip Vana, Glenn Carver, Irina Sandu and Maike Ahlgrimm. In addition, we would like to thank the OCS and GTMBA Project Office of NOAA/PMEL for providing measurements at the PAPA and PIRATA buoys, the ACAS team under the lead of Michael Tjernström for the observational data and Georgia Sotiropoulou for providing the LES data.

Geosci. Model Dev. Discuss., https://doi.org/10.5194/gmd-2018-66
Manuscript under review for journal Geosci. Model Dev.
Discussion started: 20 March 2018

6 Code and data availability

The model source code is available from the EC-Earth development portal:

svn checkout https://svn.ec-earth.org/ecearth3/branches/development/2016/r2740-coupled-SCM r2740-coupled-SCM.

More information and example data can be found on the EC-Earth AOSCM wiki page: https://dev.ec-earth.org/projects/ecearth3/wiki/Single_Column_Coupled_EC-Earth.

References

Baas, P., Bosveld, F., Lenderink, G., van Meijgaard, E., and Holtslag, A. A. M.: How to design single-column model experiments for comparison with observed nocturnal low-level jets, Quarterly Journal of the Royal Meteorological Society, 136, 671–684, https://doi.org/10.1002/qj.592, http://dx.doi.org/10.1002/qj.592, 2010.

Balmaseda, M. A., Mogensen, K., and Weaver, A. T.: Evaluation of the ECMWF ocean reanalysis system ORAS4, Quarterly Journal of the Royal Meteorological Society, 139, 1132–1161, https://doi.org/10.1002/qj.2063, http://dx.doi.org/10.1002/qj.2063, 2013.

Balsamo, G., Beljaars, A., Scipal, K., Viterbo, P., van den Hurk, B., Hirschi, M., and Betts, A. K.: A Revised Hydrology for the ECMWF Model: Verification from Field Site to Terrestrial Water Storage and Impact in the Integrated Forecast System, Journal of Hydrometeorology, 10, 623–643, https://doi.org/10.1175/2008JHM1068.1, http://dx.doi.org/10.1175/2008JHM1068.1, 2009.

Basu, S., Holtslag, A. A. M., Van De Wiel, B. J. H., Moene, A. F., and Steeneveld, G.-J.: An inconvenient "truth" about using sensible heat flux as a surface boundary condition in models under stably stratified regimes, Acta Geophysica, 56, 88–99, https://doi.org/10.2478/s11600-007-0038-y, http://dx.doi.org/10.2478/s11600-007-0038-y, 2008.

Beare, R. J., Macvean, M. K., Holtslag, A. A. M., Cuxart, J., Esau, I., Golaz, J.-C., Jimenez, M. A., Khairoutdinov, M., Kosovic, B., Lewellen, D., Lund, T. S., Lundquist, J. K., Mccabe, A., Moene, A. F., Noh, Y., Raasch, S., and Sullivan, P.: An Intercomparison of Large-Eddy Simulations of the Stable Boundary Layer, Boundary-Layer Meteorology, 118, 247–272, https://doi.org/10.1007/s10546-004-2820-6, https://doi.org/10.1007/s10546-004-2820-6, 2006.

Bechtold, P., Redelsperger, J.-L., Beau, I., Blackburn, M., Brinkop, S., Grandper, J.-Y., Grant, A., Gregory, D., Guichard, F., How, C., and Ioannidou, E.: A GCSS model intercomparison for a tropical squall line observed during toga-coare. II: Intercomparison of single-column models and a cloud-resolving model, Quarterly Journal of the Royal Meteorological Society, 126, 865–888, https://doi.org/10.1002/qj.49712656405, http://dx.doi.org/10.1002/qj.49712656405, 2000.

Betts, A. K. and Miller, M. J.: A new convective adjustment scheme. Part II: Single column tests using GATE wave, BOMEX, ATEX and arctic air-mass data sets, Quarterly Journal of the Royal Meteorological Society, 112, 693–709, https://doi.org/10.1002/qj.49711247308, http://dx.doi.org/10.1002/qj.49711247308, 1986.

Bosveld, F. C., Baas, P., Steeneveld, G.-J., Holtslag, A. A. M., Angevine, W. M., Bazile, E., de Bruijn, E. I. F., Deacu, D., Edwards, J. M., Ek, M., Larson, V. E., Pleim, J. E., Raschendorfer, M., and Svensson, G.: The Third GABLS Intercomparison Case for Evaluation Studies of Boundary-Layer Models. Part B: Results and Process Understanding, Boundary-Layer Meteorology, 152, 157–187, https://doi.org/10.1007/s10546-014-9919-1, https://doi.org/10.1007/s10546-014-9919-1, 2014.

Bourassa, M. A., Gille, S. T., Bitz, C., Carlson, D., Cerovecki, I., Clayson, C. A., Cronin, M. F., Drennan, W. M., Fairall, C. W., Hoffman, R. N., Magnusdottir, G., Pinker, R. T., Renfrew, I. A., Serreze, M., Speer, K., Talley, L. D., and Wick, G. A.: High-Latitude Ocean and Sea Ice Surface Fluxes: Challenges for Climate Research, Bulletin of the American Meteorological Society, 94, 403–423, https://doi.org/10.1175/BAMS-D-11-00244.1, http://dx.doi.org/10.1175/BAMS-D-11-00244.1, 2013.

Bourlès, B., Lumpkin, R., McPhaden, M. J., Hernandez, F., Nobre, P., Campos, E., Yu, L., Planton, S., Busalacchi, A., Moura, A. D., Servain, J., and Trotte, J.: THE PIRATA PROGRAM, Bulletin of the American Meteorological Society, 89, 1111–1126, https://doi.org/10.1175/2008BAMS2462.1, 2008.

Bretherton, C. S., Krueger, S. K., Wyant, M. C., Bechtold, P., Van Meijgaard, E., Stevens, B., and Teixeira, J.: A GCSS Boundary-Layer Cloud Model Intercomparison Study Of The First Astex Lagrangian Experiment, Boundary-Layer Meteorology, 93, 341–380, https://doi.org/10.1023/A:1002005429969, https://doi.org/10.1023/A:1002005429969, 1999.

Breugem, W.-P., Chang, P., Jang, C., Mignot, J., and Hazeleger, W.: Barrier layers and tropical Atlantic SST biases in coupled GCMs, Tellus A: Dynamic Meteorology and Oceanography, 60, 885–897, https://doi.org/10.1111/j.1600-0870.2008.00343.x, https://doi.org/10.1111/j.1600-0870.2008.00343.x, 2008.

Clayson, C. A. and Chen, A.: Sensitivity of a Coupled Single-Column Model in the Tropics to Treatment of the Interfacial Parameterizations, Journal of Climate, 15, 1805–1831, https://doi.org/10.1175/1520-0442(2002)015<1805:SOACSC>2.0.CO;2, http://dx.doi.org/10.1175/1520-0442(2002)015<1805:SOACSC>2.0.CO;2, 2002.

Cuxart, J., Holtslag, A. A. M., Beare, R. J., Bazile, E., Beljaars, A., Cheng, A., Conangla, L., Ek, M., Freedman, F., Hamdi, R., Kerstein, A., Kitagawa, H., Lenderink, G., Lewellen, D., Mailhot, J., Mauritsen, T., Perov, V., Schayes, G., Steeneveld, G.-J., Svensson, G., Taylor, P., Weng, W., Wunsch, S., and Xu, K.-M.: Single-Column Model Intercomparison for a Stably Stratified Atmospheric Boundary Layer, Boundary-Layer Meteorology, 118, 273–303, https://doi.org/10.1007/s10546-005-3780-1, https://doi.org/10.1007/s10546-005-3780-1, 2006.

Day, J. J., Svensson, G., Brooks, I. M., Bitz, C., Broman, L., Carver, G., Chevallier, M., Goessling, H., Hartung, K., Jung, T., Kay, J. E., Kolstad, E. W., Perovich, D., Screen, J., Siemen, S., and Váňa, F.: The Abisko Polar Prediction School, Bulletin of the American Meteorological Society, 98, 445–447, https://doi.org/10.1175/BAMS-D-16-0119.1, https://doi.org/10.1175/BAMS-D-16-0119.1, 2017.

de Roode, S. R., Sandu, I., van der Dussen, J. J., Ackerman, A. S., Blossey, P., Jarecka, D., Lock, A., Siebesma, A. P., and Stevens, B.: Large-Eddy Simulations of EUCLIPSE–GASS Lagrangian Stratocumulus-to-Cumulus Transitions: Mean State, Turbulence, and Decoupling, Journal of the Atmospheric Sciences, 73, 2485–2508, https://doi.org/10.1175/JAS-D-15-0215.1, https://doi.org/10.1175/JAS-D-15-0215.1, 2016.

Dee, D. P., Uppala, S. M., Simmons, A. J., Berrisford, P., Poli, P., Kobayashi, S., Andrae, U., Balmaseda, M. A., Balsamo, G., Bauer, P., Bechtold, P., Beljaars, A. C. M., van de Berg, L., Bidlot, J., Bormann, N., Delsol, C., Dragani, R., Fuentes, M., Geer, A. J., Haimberger, L., Healy, S. B., Hersbach, H., Hólm, E. V., Isaksen, L., Kållberg, P., Köhler, M., Matricardi, M., McNally, A. P., Monge-Sanz, B. M., Morcrette, J.-J., Park, B.-K., Peubey, C., de Rosnay, P., Tavolato, C., Thépaut, J.-N., and Vitart, F.: The ERA-Interim reanalysis: configuration and performance of the data assimilation system, Quart. J. Roy. Meteor. Soc., 137, 553–597, https://doi.org/10.1002/qj.828, http://dx.doi.org/10.1002/qj.828, 2011.

Deppenmeier, A.-L., Haarsma, R. J., and Hazeleger, W.: Ocean mixing and cloud feedbacks linked to tropical Atlantic SST Variability, in preparation, 2018.

Egger, J. and Schmid, S.: Elimination of spurious inertial oscillations in boundary-layer models with time-dependent geostrophic winds, Boundary-Layer Meteorology, 43, 393–402, https://doi.org/10.1007/BF00121715, http://dx.doi.org/10.1007/BF00121715, 1988.

Gaspar, P., Grégoris, Y., and Lefevre, J.-M.: A simple eddy kinetic energy model for simulations of the oceanic vertical mixing: Tests at station Papa and long-term upper ocean study site, Journal of Geophysical Research: Oceans, 95, 16 179–16 193, https://doi.org/10.1029/JC095iC09p16179, http://dx.doi.org/10.1029/JC095iC09p16179, 1990.

Ghan, S., Randall, D., Xu, K.-M., Cederwall, R., Cripe, D., Hack, J., Iacobellis, S., Klein, S., Krueger, S., Lohmann, U., Pedretti, J., Robock, A., Rotstayn, L., Somerville, R., Stenchikov, G., Sud, Y., Walker, G., Xie, S., Yio, J., and Zhang, M.: A comparison of single column model simulations of summertime midlatitude continental convection, Journal of Geophysical Research: Atmospheres, 105, 2091–2124, https://doi.org/10.1029/1999JD900971, http://dx.doi.org/10.1029/1999JD900971, 2000.

Giordani, H., Caniaux, G., and Voldoire, A.: Intraseasonal mixed-layer heat budget in the equatorial Atlantic during the cold tongue development in 2006, Journal of Geophysical Research: Oceans, 118, 650–671, 2013.

Goyette, S. and Perroud, M.: Interfacing a one-dimensional lake model with a single-column atmospheric model: Application to the deep Lake Geneva, Switzerland, Water Resources Research, 48, n/a–n/a, https://doi.org/10.1029/2011WR011223, http://dx.doi.org/10.1029/2011WR011223, 2012.

Guichard, F., Petch, J. C., Redelsperger, J.-L., Bechtold, P., Chaboureau, J.-P., Cheinet, S., Grabowski, W., Grenier, H., Jones, C. G., Köhler, M., Piriou, J.-M., Tailleux, R., and Tomasini, M.: Modelling the diurnal cycle of deep precipitating convection over land with cloud-resolving models and single-column models, Quarterly Journal of the Royal Meteorological Society, 130, 3139–3172, https://doi.org/10.1256/qj.03.145, http://dx.doi.org/10.1256/qj.03.145, 2004.

Hack, J. J. and Pedretti, J. A.: Assessment of Solution Uncertainties in Single-Column Modeling Frameworks, Journal of Climate, 13, 352–365, https://doi.org/10.1175/1520-0442(2000)013<0352:AOSUIS>2.0.CO;2, http://dx.doi.org/10.1175/1520-0442(2000)013<0352:AOSUIS>2.0.CO;2, 2000.

Hazeleger, W. and Haarsma, R. J.: Sensitivity of tropical Atlantic climate to mixing in a coupled ocean–atmosphere model, Climate dynamics, 25, 387–399, 2005.

Hazeleger, W., Severijns, C., Semmler, T., Ştefănescu, S., Yang, S., Wang, X., Wyser, K., Dutra, E., Baldasano, J. M., Bintanja, R., Bougeault, P., Caballero, R., Ekman, A. M. L., Christensen, J. H., van den Hurk, B., Jimenez, P., Jones, C., Kållberg, P., Koenigk, T., McGrath, R., Miranda, P., Noije, T. V., Palmer, T., Parodi, J. A., Schmith, T., Selten, F., Storelvmo, T., Sterl, A., Tapamo, H., Vancoppenolle, M., Viterbo, P., and Willén, U.: EC-Earth: A Seamless Earth-System Prediction Approach in Action, Bull. Am. Meteorol. Soc., 91, 1357–1363, https://doi.org/10.1175/2010BAMS2877.1, http://dx.doi.org/10.1175/2010BAMS2877.1, 2010.

Hazeleger, W., Wang, X., Severijns, C., Ştefănescu, S., Bintanja, R., Sterl, A., Wyser, K., Semmler, T., Yang, S., van den Hurk, B., van Noije, T., van der Linden, E., and van der Wiel, K.: EC-Earth V2.2: description and validation of a new seamless earth system prediction model, Clim. Dyn., 39, 2611–2629, https://doi.org/10.1007/s00382-011-1228-5, http://dx.doi.org/10.1007/s00382-011-1228-5, 2012.

Holtslag, B.: Preface: GEWEX atmospheric boundary-layer study (GABLS) on stable boundary layers, Boundary-Layer Meteorology, 118, 243–246, 2006.

Hourdin, F., Mauritsen, T., Gettelman, A., Golaz, J.-C., Balaji, V., Duan, Q., Folini, D., Ji, D., Klocke, D., Qian, Y., Rauser, F., Rio, C., Tomassini, L., Watanabe, M., and Williamson, D.: The Art and Science of Climate Model Tuning, Bulletin of the American Meteorological Society, 98, 589–602, https://doi.org/10.1175/BAMS-D-15-00135.1, https://doi.org/10.1175/BAMS-D-15-00135.1, 2017.

Hummels, R., Dengler, M., and Bourlès, B.: Seasonal and regional variability of upper ocean diapycnal heat flux in the Atlantic cold tongue, Progress in Oceanography, 111, 52 – 74, https://doi.org/https://doi.org/10.1016/j.pocean.2012.11.001, http://www.sciencedirect.com/science/article/pii/S0079661112001607, 2013.

Klein, S. A., McCoy, R. B., Morrison, H., Ackerman, A. S., Avramov, A., Boer, G. d., Chen, M., Cole, J. N. S., Del Genio, A. D., Falk, M., Foster, M. J., Fridlind, A., Golaz, J.-C., Hashino, T., Harrington, J. Y., Hoose, C., Khairoutdinov, M. F., Larson, V. E., Liu, X., Luo, Y., McFarquhar, G. M., Menon, S., Neggers, R. A. J., Park, S., Poellot, M. R., Schmidt, J. M., Sednev, I., Shipway, B. J., Shupe, M. D., Spangenberg, D. A., Sud, Y. C., Turner, D. D., Veron, D. E., Salzen, K. v., Walker, G. K., Wang, Z., Wolf, A. B., Xie, S., Xu, K.-M., Yang, F., and Zhang, G.: Intercomparison of model simulations of mixed-phase clouds observed during the ARM Mixed-Phase Arctic Cloud Experiment. I: single-layer cloud, Quarterly Journal of the Royal Meteorological Society, 135, 979–1002, https://doi.org/10.1002/qj.416, http://dx.doi.org/10.1002/qj.416, 2009.

Kraus, E. B. and Turner, J. S.: A one-dimensional model of the seasonal thermocline II. The general theory and its consequences, Tellus, 19, 98–106, https://doi.org/10.3402/tellusa.v19i1.9753, https://doi.org/10.3402/tellusa.v19i1.9753, 1967.

Large, W. G., McWilliams, J. C., and Doney, S. C.: Oceanic vertical mixing: A review and a model with a nonlocal boundary layer parameterization, Reviews of Geophysics, 32, 363–403, https://doi.org/10.1029/94RG01872, http://dx.doi.org/10.1029/94RG01872, 1994.

Lecomte, O., Fichefet, T., Massonnet, F., and Vancoppenolle, M.: Benefits from representing snow properties and related processes in coupled ocean–sea ice models, Ocean Modelling, 87, 81 – 85, https://doi.org/http://doi.org/10.1016/j.ocemod.2014.11.005, http://www.sciencedirect.com/science/article/pii/S1463500314001723, 2015.

Lemarié, F., Blayo, E., and Debreu, L.: Analysis of Ocean-atmosphere Coupling Algorithms: Consistency and Stability, Procedia Computer Science, 51, 2066 – 2075, https://doi.org/https://doi.org/10.1016/j.procs.2015.05.473, http://www.sciencedirect.com/science/article/pii/S1877050915012818, international Conference On Computational Science, ICCS 2015, 2015.

Lenderink, G., Siebesma, A. P., Cheinet, S., Irons, S., Jones, C. G., Marquet, P., üLLER, F. M., Olmeda, D., Calvo, J., Sánchez, E., and Soares, P. M. M.: The diurnal cycle of shallow cumulus clouds over land: A single-column model intercomparison study, Quarterly Journal of the Royal Meteorological Society, 130, 3339–3364, https://doi.org/10.1256/qj.03.122, http://dx.doi.org/10.1256/qj.03.122, 2004.

Ling, T., Xu, M., Liang, X.-Z., Wang, J. X. L., and Noh, Y.: A multilevel ocean mixed layer model resolving the diurnal cycle: Development and validation, Journal of Advances in Modeling Earth Systems, 7, 1680–1692, https://doi.org/10.1002/2015MS000476, http://dx.doi.org/10.1002/2015MS000476, 2015.

Lübbecke, J. F., Böning, C. W., Keenlyside, N. S., and Xie, S.-P.: On the connection between Benguela and equatorial Atlantic Niños and the role of the South Atlantic Anticyclone, Journal of Geophysical Research: Oceans, 115, 2010.

Madec, G.: NEMO ocean engine. Note du Pole de modélisation, Version 3.6 27 ISSN No 1288-1619, Institut Pierre-Simon Laplace (IPSL), France, 2016.

NASA Goddard Space Flight Center, Ocean Ecology Laboratory, O. B. P. G.: Sea-viewing Wide Field-of-view Sensor (SeaWiFS) Ocean Color Data, NASA OB.DAAC, Greenbelt, MD, USA, 2014.

Niiler, P. and Kraus, E. B.: One-dimensional models of the upper ocean, in: Modelling and Prediction of the Upper Layers of the Ocean, edited by Kraus, E. B., pp. 143–172, Pergamon, Tarrytown, N.Y., 1977.

Pithan, F., Ackerman, A., Angevine, W. M., Hartung, K., Ickes, L., Kelley, M., Medeiros, B., Sandu, I., Steeneveld, G.-J., Sterk, H. A. M., Svensson, G., Vaillancourt, P. A., and Zadra, A.: Select strengths and biases of models in representing the Arctic winter boundary layer over sea ice: the Larcform 1 single column model intercomparison, Journal of Advances in Modeling Earth Systems, 8, 1345–1357, https://doi.org/10.1002/2016MS000630, http://dx.doi.org/10.1002/2016MS000630, 2016.

Price, J. F., Weller, R. A., and Pinkel, R.: Diurnal cycling: Observations and models of the upper ocean response to diurnal heating, cooling, and wind mixing, Journal of Geophysical Research: Oceans, 91, 8411–8427, https://doi.org/10.1029/JC091iC07p08411, http://dx.doi.org/10.1029/JC091iC07p08411, 1986.

Randall, D. A. and Cripe, D. G.: Alternative methods for specification of observed forcing in single-column models and cloud system models, Journal of Geophysical Research: Atmospheres, 104, 24 527–24 545, https://doi.org/10.1029/1999JD900765, http://dx.doi.org/10.1029/1999JD900765, 1999.

Randall, D. A., Xu, K.-m., Somerville, R. J. C., and Iacobellis, S.: Single-Column Models and Cloud Ensemble Models as Links between Observations and Climate Models, Journal of Climate, 9, 1683–1697, https://doi.org/10.1175/1520-0442(1996)009<1683:SCMACE>2.0.CO;2, http://dx.doi.org/10.1175/1520-0442(1996)009<1683:SCMACE>2.0.CO;2, 1996.

Reffray, G., Bourdalle-Badie, R., and Calone, C.: Modelling turbulent vertical mixing sensitivity using a 1-D version of NEMO, Geoscientific Model Development, 8, 69–86, https://doi.org/10.5194/gmd-8-69-2015, http://www.geosci-model-dev.net/8/69/2015/, 2015.

Rousset, C., Vancoppenolle, M., Madec, G., Fichefet, T., Flavoni, S., Barthélemy, A., Benshila, R., Chanut, J., Levy, C., Masson, S., and Vivier, F.: The Louvain-La-Neuve sea ice model LIM3.6: global and regional capabilities, Geoscientific Model Development, 8, 2991–3005, https://doi.org/10.5194/gmd-8-2991-2015, https://www.geosci-model-dev.net/8/2991/2015/, 2015.

Savre, J., Ekman, A. M. L., and Svensson, G.: Technical note: Introduction to MIMICA, a large-eddy simulation solver for cloudy planetary boundary layers, Journal of Advances in Modeling Earth Systems, 6, 630–649, https://doi.org/10.1002/2013MS000292, http://dx.doi.org/10.1002/2013MS000292, 2014.

Servain, J., Busalacchi, A. J., McPhaden, M. J., Moura, A. D., Reverdin, G., Vianna, M., and Zebiak, S. E.: A pilot research moored array in the tropical Atlantic (PIRATA), Bulletin of the American Meteorological Society, 79, 2019–2031, 1998.

Sigg, R. and Svensson, G.: Three-dimensional simulation of the ASTEX Lagrangian 1 field experiment with a regional numerical weather prediction model, Quarterly Journal of the Royal Meteorological Society, 130, 707–724, https://doi.org/10.1256/qj.02.209, http://dx.doi.org/10.1256/qj.02.209, 2004.

Sotiropoulou, G., Tjernström, M., Savre, J., Ekman, A. M. L., Hartung, K., and Sedlar, J.: Large Eddy Simulation of warm-air advection and air-mass transformation in the summer Arctic, submitted to QJRMS, 2018.

Spengler, T., Renfrew, I. A., Terpstra, A., Tjernström, M., Screen, J., Brooks, I. M., Carleton, A., Chechin, D., Chen, L., Doyle, J., Esau, I., Hezel, P. J., Jung, T., Kohyama, T., Lüpkes, C., McCusker, K. E., Nygård, T., Sergeev, D., Shupe, M. D., Sodemann, H., and Vihma, T.: High-Latitude Dynamics of Atmosphere–Ice–Ocean Interactions, Bulletin of the American Meteorological Society, 97, ES179–ES182, https://doi.org/10.1175/BAMS-D-15-00302.1, http://dx.doi.org/10.1175/BAMS-D-15-00302.1, 2016.

Sterk, H. A. M., Steeneveld, G. J., and Holtslag, A. A. M.: The role of snow-surface coupling, radiation, and turbulent mixing in modeling a stable boundary layer over Arctic sea ice, Journal of Geophysical Research: Atmospheres, 118, 1199–1217, https://doi.org/10.1002/jgrd.50158, http://dx.doi.org/10.1002/jgrd.50158, 2013.

Svensson, G., Holtslag, A. A. M., Kumar, V., Mauritsen, T., Steeneveld, G. J., Angevine, W. M., Bazile, E., Beljaars, A., de Bruijn, E. I. F., Cheng, A., Conangla, L., Cuxart, J., Ek, M., Falk, M. J., Freedman, F., Kitagawa, H., Larson, V. E., Lock, A., Mailhot, J., Masson, V., Park, S., Pleim, J., Söderberg, S., Weng, W., and Zampieri, M.: Evaluation of the Diurnal Cycle in the Atmospheric Boundary Layer Over Land as Represented by a Variety of Single-Column Models: The Second GABLS Experiment, Boundary-Layer Meteorology, 140, 177–206, https://doi.org/10.1007/s10546-011-9611-7, https://doi.org/10.1007/s10546-011-9611-7, 2011.

Tjernström, M., Shupe, M. D., Brooks, I. M., Persson, P. O. G., Prytherch, J., Salisbury, D. J., Sedlar, J., Achtert, P., Brooks, B. J., Johnston, P. E., Sotiropoulou, G., and Wolfe, D.: Warm-air advection, air mass transformation and fog causes rapid ice melt, Geophysical Research Letters, 42, 5594–5602, https://doi.org/10.1002/2015GL064373, http://dx.doi.org/10.1002/2015GL064373, 2015GL064373, 2015.

Toniazzo, T. and Woolnough, S.: Development of warm SST errors in the southern tropical Atlantic in CMIP5 decadal hindcasts, Climate dynamics, 43, 2889–2913, 2014.

Valcke, S.: OASIS3 User Guide, Tech. rep., CERFACS, Toulouse, France, 2006.

Voldoire, A., Demissie, T., Deppenmeier, A.-L., Exarchou, E., Frauen, C., Goubanova, K., Keenlyside, N., Koseki, S., Prodhomme, C., Sanchez-Gomez, E., Shen, M.-L., Shonk, J., Toniazzo, T., and Taore, A.-K.: Development of warm SST errors in the southern tropical Atlantic in CMIP5 decadal hindcasts, in preparation, 2018.

West, A. E., McLaren, A. J., Hewitt, H. T., and Best, M. J.: The location of the thermodynamic atmosphere–ice interface in fully coupled models – a case study using JULES and CICE, Geoscientific Model Development, 9, 1125–1141, https://doi.org/10.5194/gmd-9-1125-2016, http://www.geosci-model-dev.net/9/1125/2016/, 2016.

Williams, P. D.: Climatic impacts of stochastic fluctuations in air–sea fluxes, Geophysical Research Letters, 39, n/a–n/a, https://doi.org/10.1029/2012GL051813, http://dx.doi.org/10.1029/2012GL051813, l10705, 2012.

Xie, S.-P. and Carton, J. A.: Tropical Atlantic Variability: Patterns, Mechanisms, and Impacts, in: Earth's Climate, pp. 121–142, American Geophysical Union, https://doi.org/10.1029/147GM07, 2004.

Geosci. Model Dev. Discuss., https://doi.org/10.5194/gmd-2018-66
Manuscript under review for journal Geosci. Model Dev.
Discussion started: 20 March 2018

Geoscientific Model Development Discussions

Figure 1. Flow chart of the OIFS model

Geosci. Model Dev. Discuss., https://doi.org/10.5194/gmd-2018-66
Manuscript under review for journal Geosci. Model Dev.
Discussion started: 20 March 2018

Geoscientific Model Development Discussions

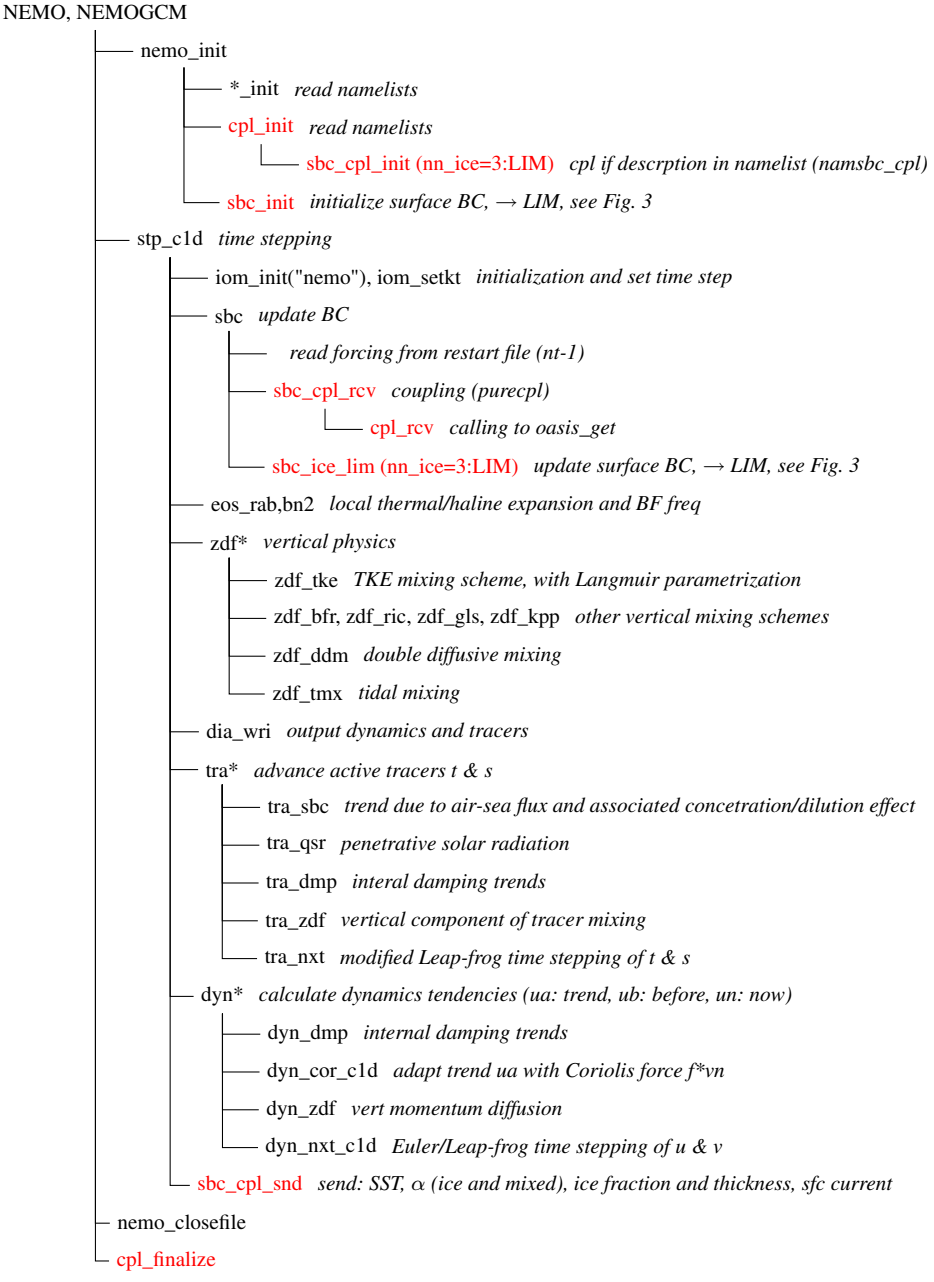

Figure 2. Flow chart of the NEMO model

Geosci. Model Dev. Discuss., https://doi.org/10.5194/gmd-2018-66
Manuscript under review for journal Geosci. Model Dev.
Discussion started: 20 March 2018

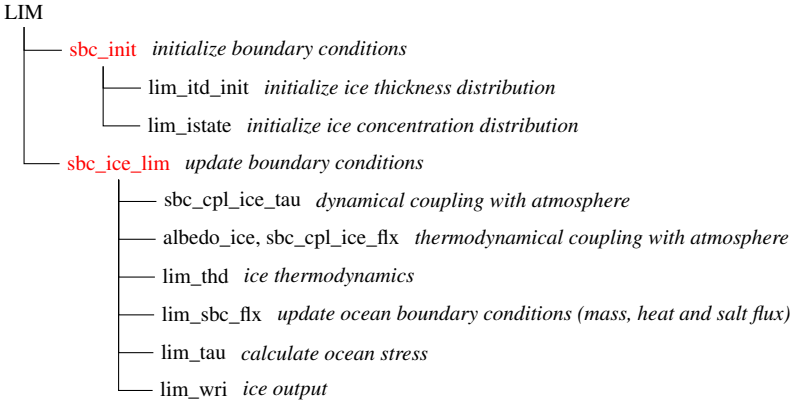

Figure 3. Flow chart of the LIM model, part of the NEMO model if (nn_ice=3:LIM) in sbcice_lim (stp_c1d)

Geosci. Model Dev. Discuss., https://doi.org/10.5194/gmd-2018-66
Manuscript under review for journal Geosci. Model Dev.
Discussion started: 20 March 2018

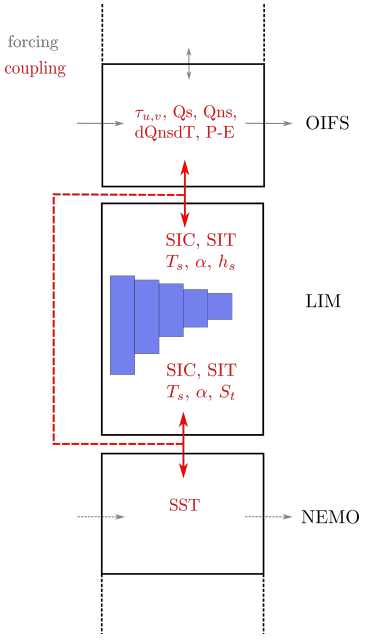

Figure 4. Schematic of coupling variables exchanged between the model components. In the polar environment all red lines represent the coupling (dashed and full) and without sea-ice coupling reduces to the dashed line. From the atmosphere the horizontal wind stress $\tau_{u,v}$, the solar flux Q_s, the non-solar fluxes Q_{ns} and precipitation minus evaporation $P-E$ are passed to the ocean. In the presence of ice, the temperature sensitivity of the non-solar fluxes $dQ_{ns}dT$ is coupled as well. The ocean model sends the sea-surface temperature SST and in the presence of sea-ice the aggregated sea-ice concentration SIC, sea-ice thickness SIT, surface temperature T_s, surface albedo α and the snow thickness h_s. In a coupled simulation with sea-ice the ocean also receives the ice parameters SIC, SIT, T_s and α and in addition the rate of change of the sea-ice thickness S_t.

Geosci. Model Dev. Discuss., https://doi.org/10.5194/gmd-2018-66
Manuscript under review for journal Geosci. Model Dev.
Discussion started: 20 March 2018

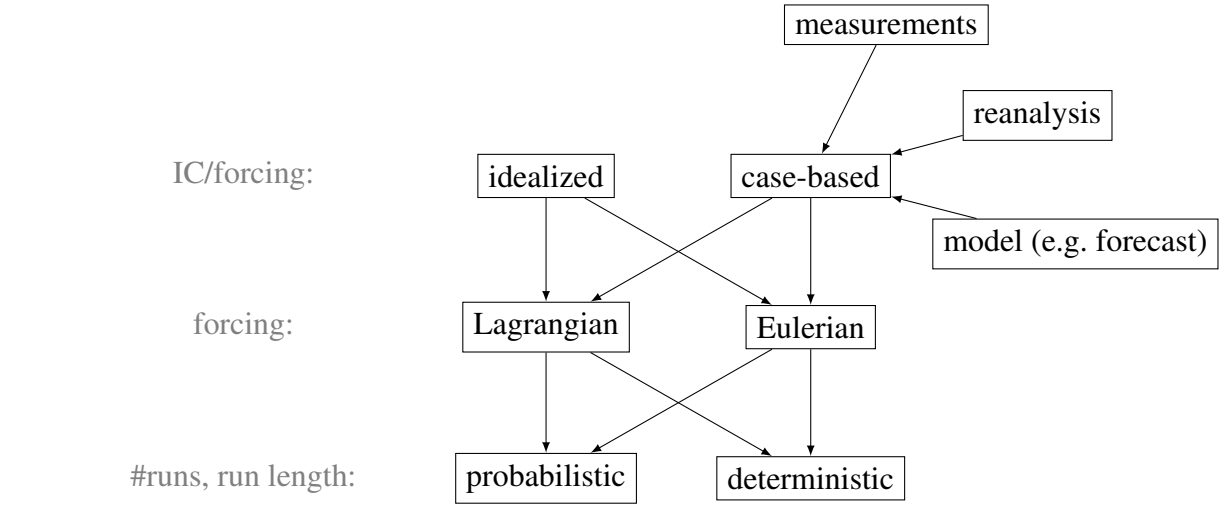

Figure 5. How to set up an SCM experiment

Table 1. Surface RMSE after 28 days evaluated with respect to PAPA mooring measurements. Suffix of simulation based on atmospheric forcing frequency. Extra nudging information in parenthesis.

	AOSCM-6h	ASCM-6h	AOSCM-3h	AOSCM-6h (uvrel, τ =1h)	AOSCM-6h (uvTqrel, τ =6h)
T_{2m} [°C]	0.9 ± 0.2	0.8 ± 0.2	0.8 ± 0.2	0.9 ± 0.2	0.8 ± 0.2
SST [°C]	0.6 ± 0.3	0.4 ± 0.1	0.4 ± 0.3	0.4 ± 0.3	0.4 ± 0.2
SW rad [Wm^{-2}]	84 ± 27	82 ± 37	77 ± 34	78 ± 35	77 ± 34
LW rad [Wm^{-2}]	24 ± 5	24 ± 5	23 ± 5	23 ± 5	24 ± 4
SH flux[Wm^{-2}]	13 ± 7	13 ± 8	11 ± 5	12 ± 6	12 ± 7
LH flux [Wm^{-2}]	26 ± 13	28 ± 13	22 ± 10	24 ± 10	27 ± 13
u_{10m} [ms^{-1}]	2.0 ± 0.8	2.1 ± 0.8	1.5 ± 0.3	1.3 ± 0.3	1.9 ± 0.7

Table 2. Atmospheric RMSE after 28 days evaluated with respect to ERA-Interim fields

	AOSCM-6h	ASCM-6h	AOSCM-3h	AOSCM-6h (uvrel, τ =1h)	AOSCM-6h (uvTqrel, τ =6h)
T [°C], to 1km	1.7 ± 0.7	1.6 ± 0.6	1.3 ± 0.7	1.6 ± 0.5	1.3 ± 0.4
T [°C], to 3km	2.5 ± 1.4	2.5 ± 1.4	1.6 ± 0.7	2.4 ± 1.3	1.3 ± 0.2
q [$g\ kg^{-1}$], to 1km	7 ± 3	7 ± 2	5 ± 3	7 ± 3	6 ± 2
q [$g\ kg^{-1}$], to 3km	9 ± 4	10 ± 5	6 ± 3	9 ± 4	7 ± 2
wind [ms^{-1}], to 1km	3.2 ± 1.4	3.2 ± 1.4	1.8 ± 0.5	0.5 ± 0.2	2.7 ± 1.2
wind [ms^{-1}], to 3km	5.3 ± 1.7	5.3 ± 1.7	2.7 ± 0.9	0.5 ± 0.2	2.6 ± 1.0

Geosci. Model Dev. Discuss., https://doi.org/10.5194/gmd-2018-66
Manuscript under review for journal Geosci. Model Dev.
Discussion started: 20 March 2018

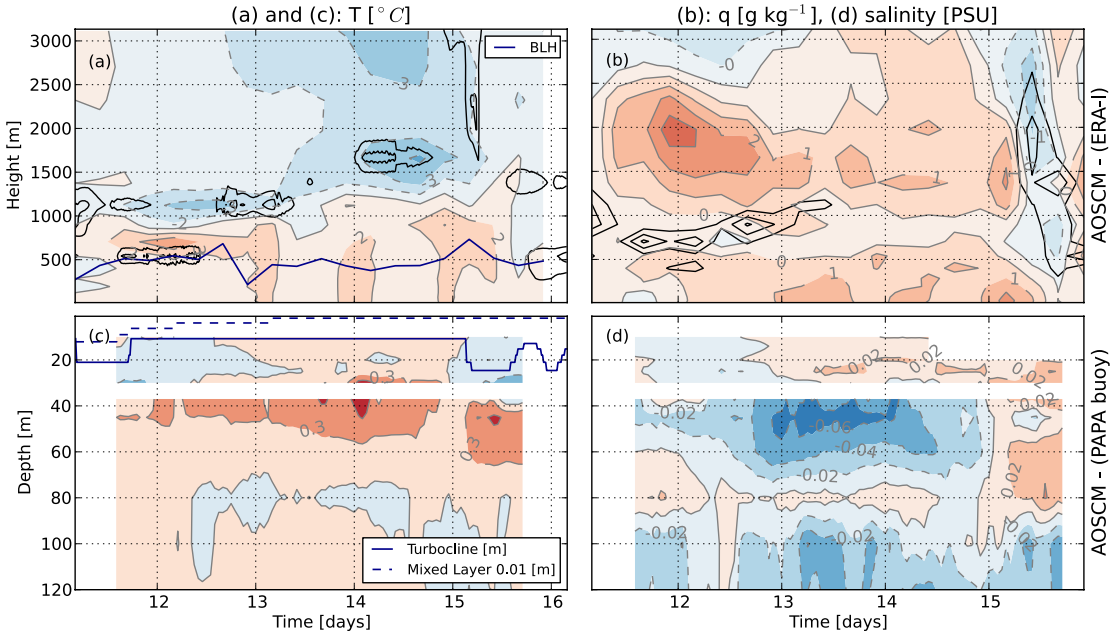

Figure 6. Coupled model biases of AOSCM-6h relative to ERA-Interim and PAPA buoy measurements for July 11-15 2014. Note that the colour contours match different values for atmosphere and ocean. White areas indicate missing buoy data. Measured temperature and salinity evolution is smoothed with a 12 h running mean to remove tidal influences not included in the model. The liquid water content, i.e. the cloud, in the model (reanalysis) is given in panel (a) ((b)) in black contours showing 0.1, 0.2 and 0.3 g kg^{-1}.

Geosci. Model Dev. Discuss., https://doi.org/10.5194/gmd-2018-66
Manuscript under review for journal Geosci. Model Dev.
Discussion started: 20 March 2018

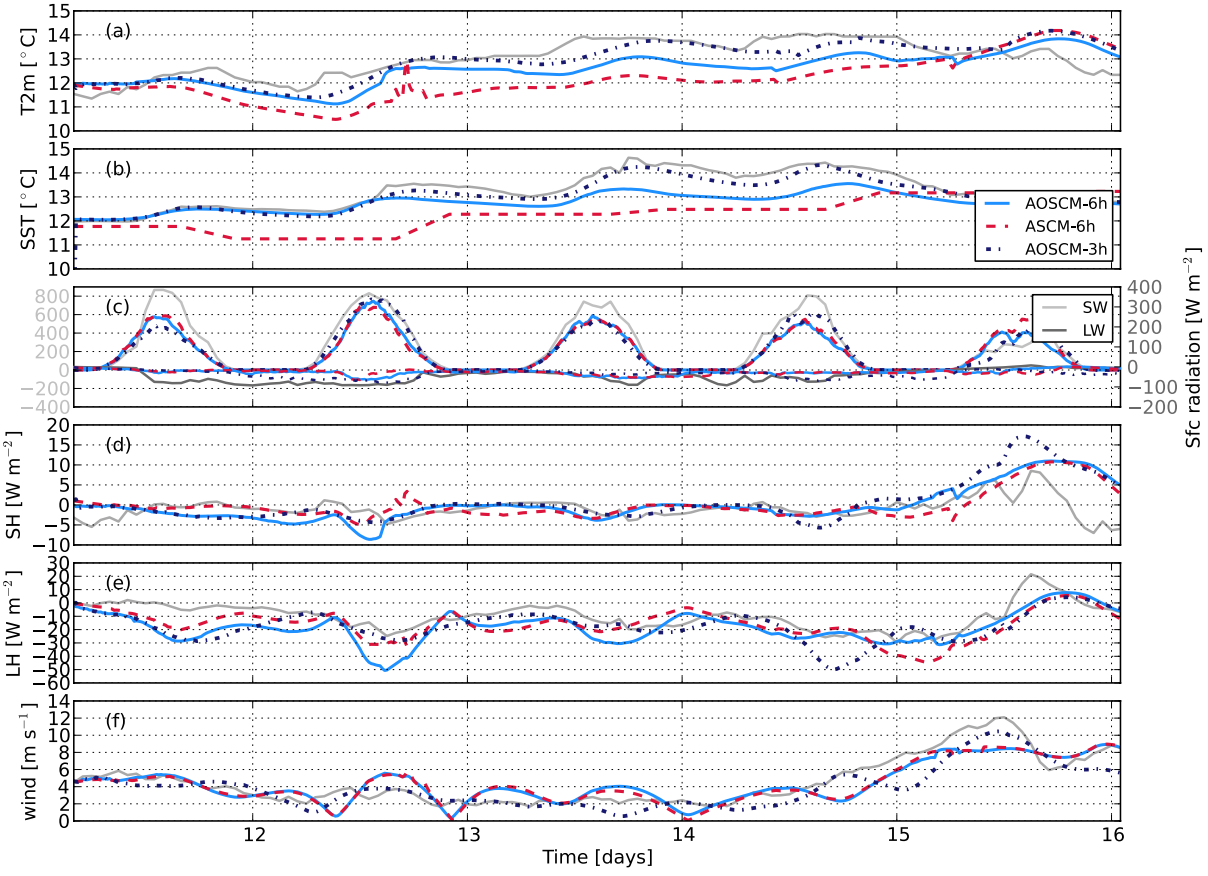

Figure 7. Model evolution at the PAPA buoy during Jul 11-15 2014 for AOSCM-6h, ASCM-6h and AOSCM-3h. Radiative fluxes are smoothed in time with a running-mean timescale of one hour. Measurements from PAPA buoy in grey. All fluxes are defined positive downward.

Geosci. Model Dev. Discuss., https://doi.org/10.5194/gmd-2018-66
Manuscript under review for journal Geosci. Model Dev.
Discussion started: 20 March 2018

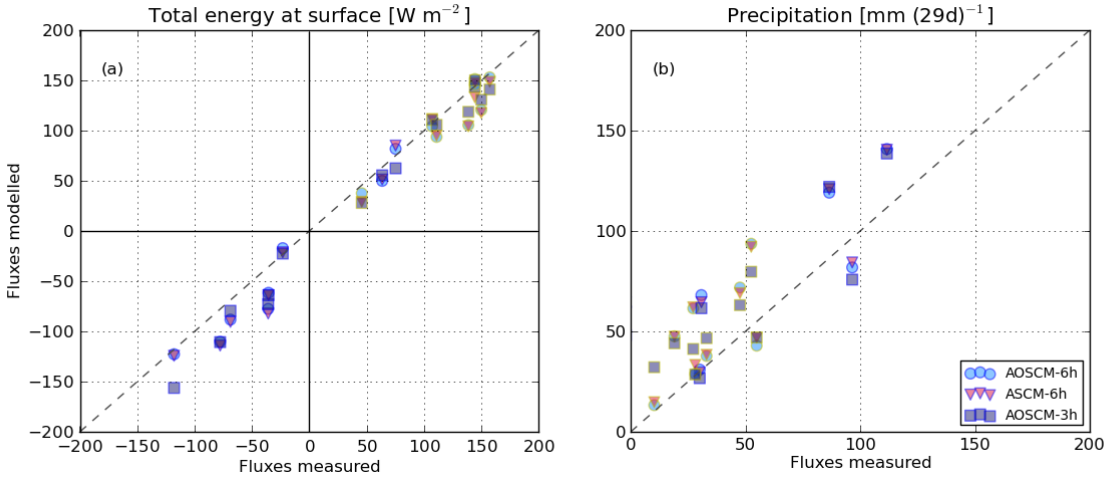

Figure 8. Accumulated fluxes, total surface energy and precipitation calculated over 29-day simulations at the PAPA mooring, compared for three main sensitivity runs AOSCM-6h, ASCM-6h and AOSCM-3h across all sixteen simulations. Symbols with a light (dark) border represent results from warm (cold) months. Modelled precipitation is filtered with the measurement hourly rain threshold of 0.2 mm h^{-1}

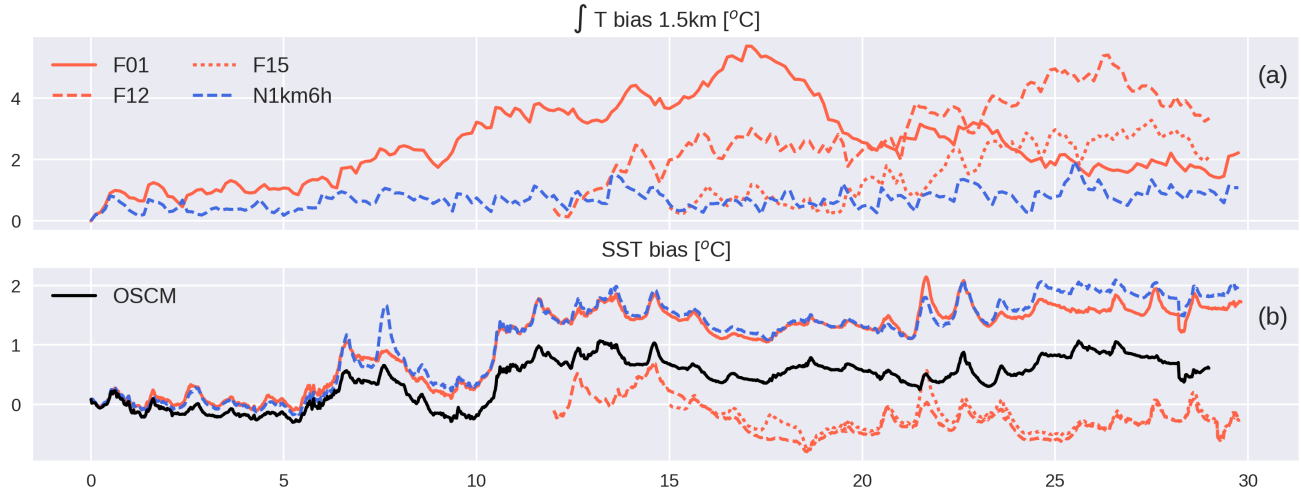

Figure 9. Atmospheric root-mean square error integrated in lower 1.5 km of the atmosphere compared to ERA-Interim and SST biases relative to PIRATA measurements for several coupled and one ocean-only simulation. Fxx show results from simulations forced with advective tendencies and initialized on day $xx = \in \{01, 12, 15\}$ of June 2014. N1km6h uses the same forcing as F01 but additionally nudging is added to horizontal wind, temperature and moisture above 1 km with $\tau = 6$ h. OSCM is an ocean-only simulation.

Geosci. Model Dev. Discuss., https://doi.org/10.5194/gmd-2018-66
Manuscript under review for journal Geosci. Model Dev.
Discussion started: 20 March 2018

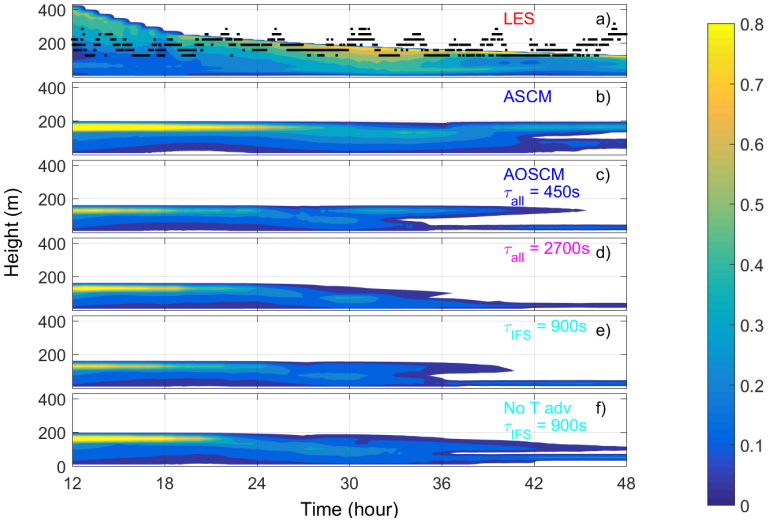

Figure 10. Time-height evolution of the simulated cloud liquid water content (g kg^{-1}) in the Arctic setup for hours 12 to 48 with a color scale that maximize at about 0.8 (g kg^{-1}) for a) LES results from Sotiropoulou et al. (2018), b) ASCM simulation with a time step of 450 s and 132 layers, c) AOSCM with time step 450 s in all components and coupling, d) AOSCM with conditions similar to EC-Earth i.e. 2700 s for all time steps and coupling, e) as in d) but with 900 s time step for the atmospheric component, and f) as in e) but with no temperature advection. Observational estimates of cloud base (red dots) and top (black dots) from ACSE are also included in a).

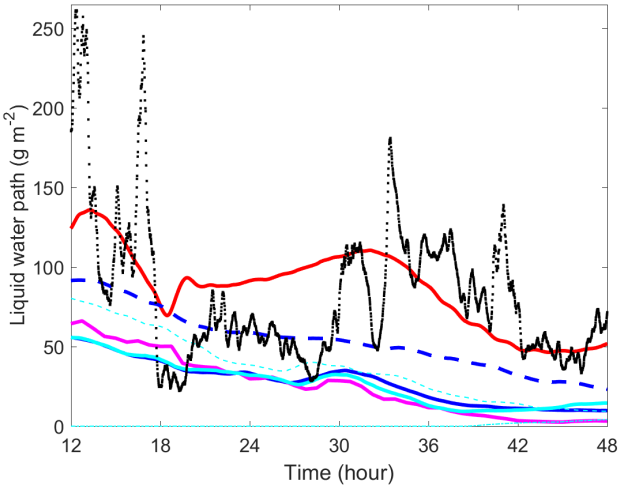

Figure 11. Liquid-water path in (g m^{-2}) for all Arctic simulations presented in Fig. 10, LES - red line, ASCM blue dashed line, AOSCM with various time steps - blue (all 450 s), magenta (all 2700 s) and cyan (IFS 900 s, other 2700 s). Also included are the results from simulations without advection of temperature (dashed cyan line) and without humidity (dash-dotted cyan thin line). Observations are shown as running averages over approximately 10 min (black dots).

Geosci. Model Dev. Discuss., https://doi.org/10.5194/gmd-2018-66
Manuscript under review for journal Geosci. Model Dev.
Discussion started: 20 March 2018

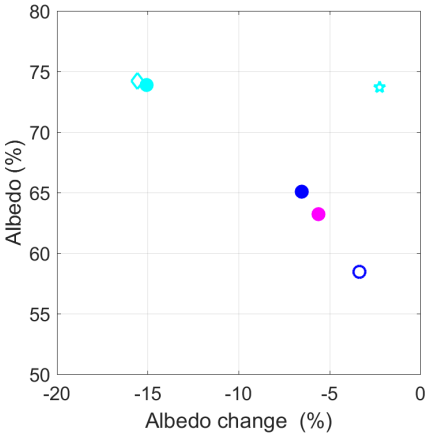

Figure 12. Mean albedo (%) change over the simulated 40 hours plotted against the mean albedo for the first simulated hour for the experiments in Fig. 10, same colors as in Fig. 11, ASCM open blue symbol, AOSCM simulations with no advection of temperature (cyan star) and no humidity advection (cyan diamond) are also included.

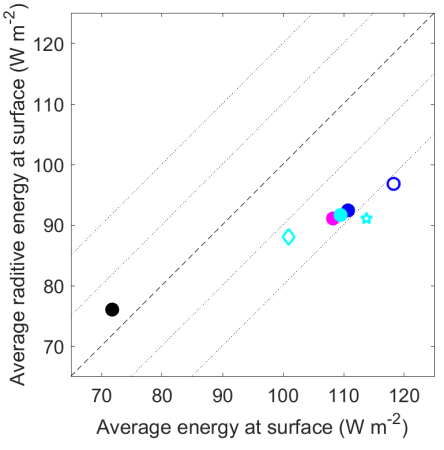

Figure 13. Average radiative energy as function of average energy received at the surface for hour 12 to 48 for the simulations (same symbols as in Fig. 12) and observations (black dot). The thin dotted lines around the 1-to-1 line represents ± 10 and 20 W m^{-2}.